STRAY LIGHT ANALYSIS OF THE

DIFFUSE INFRARED BACKGROUND EXPERIMENT (DIRBE)

Prepared by:

Robert P. Breault

Breault Research Organization, Inc.
1161 N. El Dorado Place, Suite 340
Tucson, AZ 85715

For:

NASA Goddard Space Flight Center
under Contract NAS5-27274

March 23, 1984

TABLE OF CONTENTS

LIST OF FIGURES

LIST OF TABLES

1.0 INTRODUCTION

This report discusses the straylight analysis of the Diffuse Infrared Background Experiment (DIRBE) on the Cosmic Background Explorer (COBE) Mission. From the statement of work (SOW), the purpose of DIRBE is to measure, or set upper limits on, the spectral and spatial character of the diffuse extra galactic infrared radiation. Diffuse infrared sources within our own galaxy will be measured. The required reduction of the unwanted radiation imposes severe design and operating restrictions on the DIRBE instrument. Furthermore, in order to accomplish its mission, it will operate at a multitude of wavelengths ranging from 1.25 um out to 200-300 microns. The operating bands are shown in Table 1 and the required Point

Table 1. Wavebands.

1.0	-	1.5
8.0	-	15.0
37.5	-	38.5
120.0	-	200.0
200.0	-	300.0

Source Normalized Irradiance Transmittance (PSNIT) is shown in Table 2 for

Table 2. DIRBE specifications straylight PSNIT.

Wavelength (in microns)	$\log_{10}$ PSNIT
1.5	-18
10.6	-15
100.0	-12.5

PSNIT = DETECTOR IRRADIANCE PER UNIT INCIDENT PLANE WAVE.

some of the bands. The required PSNIT's represent performance characteristics as good as any telescope yet designed.

Section 2 is a brief review of the important straylight concepts in the DIRBE design.

Section 3 will explain the model and the assumptions used in the APART analysis. It will also cover the limitations due to the scalar theory used in the analysis.

Section 4 is a detailed description of the BRDF's used. The wavelength scaling of the BRDF will also be discussed.

Section 5 will present the results of the analysis for 5 wavebands, along with the thermal emission and other results.

This will be followed by Section 6, the conclusions and recommendations, and section 7 which is a brief summary. Appendix A contains some APART input files for the DIRBE analysis, and is included with this report as an example of representative input decks. Appendix B is NASA supplied mirror BRDF data. Appendix C, supplied under separate cover, is a computer listing of all the significant input files used in the analysis.

In order to accomplish the mission, several constraints were imposed on the DIRBE instrument. First, an external and large Sunshield was designed for DIRBE and the operating conditions were set so that the Sun and the Earth would always be at 94 degrees or more from the spin axis of the observatory. This requirement meant that the energy from the Sun and Earth first had to be diffracted to get to the DIRBE instrument. By design it is even better than that. It really requires three diffractions because of the placement of additional vanes on the tip of the Sunshield, which will be shown later.

2.0 CONCEPTS

The constraints on the position of the Sun and Earth is severe but certainly allows the system optimum straylight operating conditions. Be that as it may, there is yet one more very clever straylight technique used in the DIRBE design. Even the above diffracted energy cannot directly enter the main baffle of the DIRBE instrument. The diffracted energy can only fall on a cone-like forebaffle structure that is highly polished (aluminum). The specular beam is directed out the system, and only the very large back angle scatter off the mirror-like surface can scatter into the vane structure on the main tube. The large back scatter angle yields a Bidirectional Reflectance Distribution Function (BRDF) value far lower than the best diffuse black coating. The vane structure then absorbs a significant amount of this incoming radiation. Therefore, the combined effect of the three diffracting edges, the prebaffle, and the black baffles, is the attenuation of the incoming energy from the Sun and Earth to acceptable levels.

It is the secondary sources, the Moon, Jupiter and the generally widespread diffuse space background that limits the system's performance. The basic design of the system incorporates the "optimum" straylight design features of a well designed system.

In the report, considerable attention will seem to be directed towards a single element type of system, i.e., from the source to the primary and then directly to the detector. The concept involved is that the incoming

radiation as a function of its off axis position will illuminate certain internal objects in the system. These objects we will call the "HOT" objects. The detector, on the other hand, will see from its location another set of objects that we call "critical" objects. The term critical being used here because they are the sole source of energy to the detector and are, therefore, critical to the system's performance. Ideally one would always want the two classes of objects to be distinct. But with an unvignetted field of view that is not possible when the source is in the field of view (FOV) or even when it is just near the FOV because when the source is just at the edge of the FOV, the objective is fully illuminated. Therefore, just outside the FOV most of the primary will still be illuminated. So at least that element is both a HOT object and Critical object. Furthermore, in DIRBE, for sources outside the FOV, all the direct input energy will be blocked by the field stop at the prime focus of the objective. The field stop limits the number of objects in the class of HOT objects. Nothing beyond the field stop can be illuminated by an out of field source.

The use of a field stop doesn't make a complete straylight system, because as shown in Figure 1, the detector just might, unnecessarily, be able to see through the field stop to some of these Hot objects if it weren't for the Lyot stop in the system. A Lyot stop is an aperture that is conjugate to the system's aperture. Ideally the Lyot stop is at the location of the exit aperture and is slightly undersized. Its role is to limit the number of objects that the detector can see, i.e., it limits the number of Critical objects. In the DIRBE design where both a field stop and Lyot stop are used, it is possible to have only one object, the objective (the primary in DIRBE) in both classes (Hot and Critical).

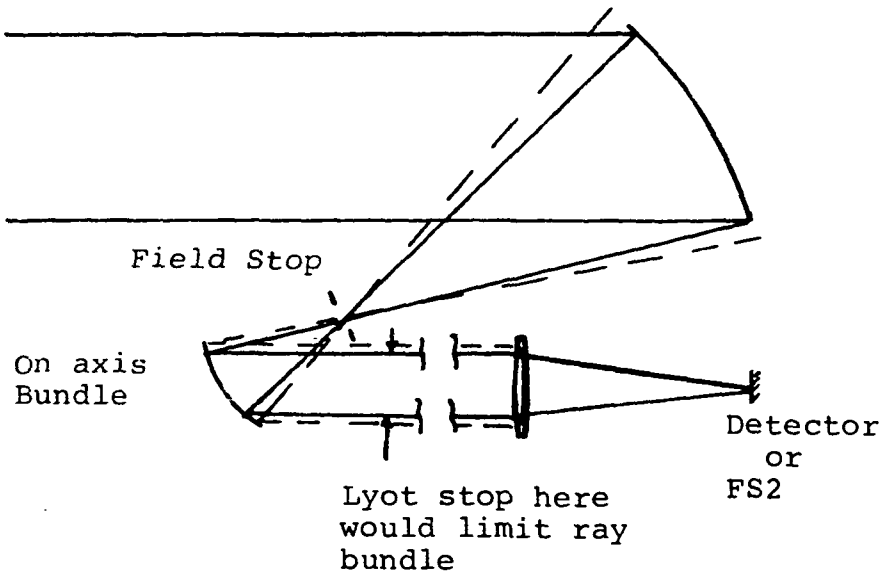

Figure 1. The detector can see through field stop.

There were two complex details of the model that deserve special attention. The first was the rectangular cavity between the first Lyot Stop and the Tertiary. A special model was developed for this type of cavity which was called a "pyramid". In DIRBE, the slopes of the walls are relatively mild and there was never any peak to the pyramid, therefore, creating a box-like shape. In the final analysis these surfaces had no measurable impact on the final results because these occur after the first field stop/Lyot stop combination and, therefore, don't receive significant amounts of power.

A second detail of the model was both more complex and, also, it had a meaningful impact on the analysis. The main baffle around and in front of the primary mirror had two major parts, one, a cylindrical tube from the entrance aperture to the primary, and second, a conical tube from the primary to the first Field Stop (FS1). These two surfaces intersected each other forming a complex junction of vane surfaces.

The new version of APART was able to model these objects as a series of five objects (10, 11,34, 17 and 38), see Figure 2. Object 10 was the short front, fully cylindrical, section. Objects 11 and 34 were also cylindrical sections but they have their lower sections sliced away to make room for object 17 and 38, (each of which had their corresponding upper sections removed). The reason that there are two cylindrical sections (11 and 34) and two conical sections (17 and 38) is that the profile of the intersection of the objects was not a straight line as shown in Figure 3. APART only has slicing planes. Hence, two objects were modeled with different slicing planes.

2.1 Primary Mirror

Let us discuss the primary mirror to see what affects the magnitude of its BRDF. In the long run it will warrant every bit of attention given to it. If the surface is to be coated, i.e., with an aluminum thin film coating, then the surface contamination at the time of the application of the thin film is extremely important, and save for recoating of the surface, its effect is irreversible. Improper coatings can cause a BRDF to unnecessarily increase by a factor of 50 if only modest attention is paid to the cleaning process.

Characteristically metal mirrors have not performed as well as their glass counterparts when rated according to their BRDF's. Sleeks seem to abound on metal mirrors to a noticeably higher degree than on glass. The measured BRDF supplied by NASA, Appendix B, seems to contradict this, but they are not necessarily representative of the general cases.

In the DIRBE instrument the straylight that reaches the detector will either be from the primary mirror or from diffraction off the apertures. If the primary is the major source of unwanted energy, then there are two ways to make improvements. The first is to do what is necessary to improve (lower) the scattering characteristics (BRDF) of the primary's surface. This

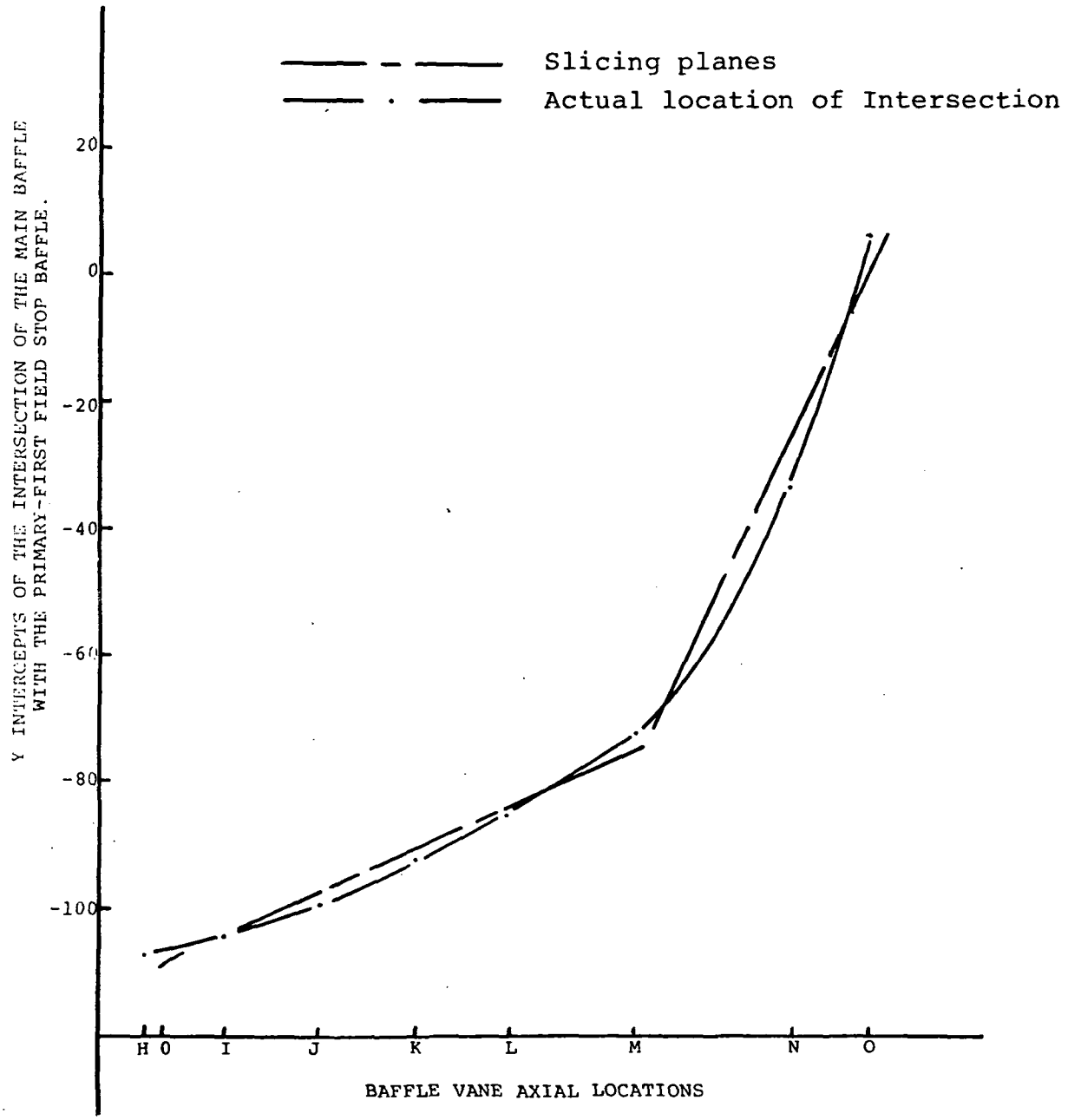

Figure 2. Locus of intersections of the main cylindrical baffle and the conical baffle converging from the primary

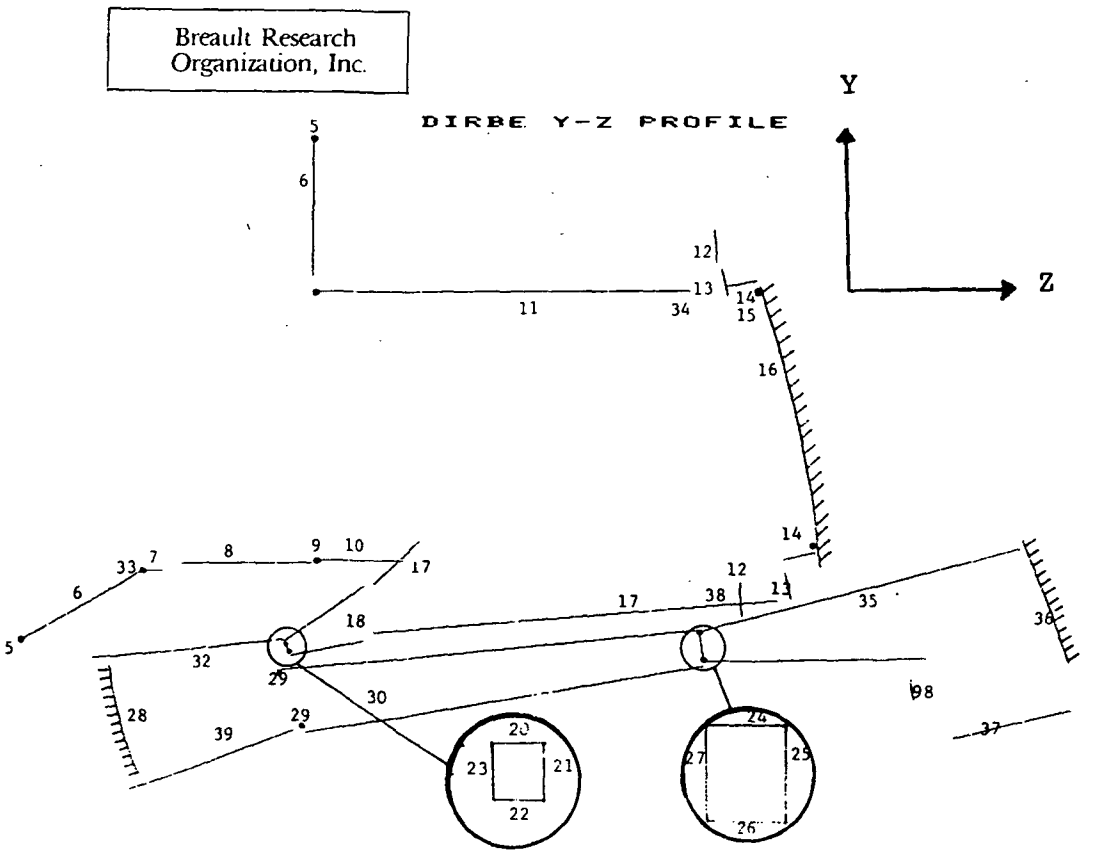

Figure 3. Profile Y-Z plane DIRBE.

involves the substrate, the degree of polish, cleaning, coating and keeping any pre-launch contamination from getting to the primary.

The second way to improve the system is to keep unwanted energy from reaching the primary. As explained above, this has already been achieved for sources at large off-axis angles. For intermediate off-axis angles the only path to the primary is via multiple scatter from the vaned main baffle. The appropriate constraint on the vane spacing is that over the range of angles of the source there be no direct path from the source to the main tubes wall that can then scatter directly to the primary. If this condition is met, then the incoming radiation should be attenuated by five or more orders of magnitude by the vanes. If not, it may be as little as only one order of attentuation. In the DIRBE design the baffles, if anything, are too close together. This over design will have only a minor detrimental effect which comes mainly from the additional edge scatter.

For small off axis angles, those that can put power directly onto the primary mirror, the only method to improve performance is to reduce the scatter off the primary. This requires both making a low scatter mirror, and then KEEPING it clean. Both will require a significant amount of effort.

2.2 Diffraction

The second source of unwanted energy is from multiple diffraction paths. One method most commonly used to beat down the diffracted energy is to baffle the diffraction from the edges. This is done in concept in DIRBE through the use of multiple Field Stops (FS), an Aperture Stop, and a Lyot Stop. In order for these multiple stops to be effective, the diffraction must be sufficiently blocked by a succeeding aperture at a conjugate image location. DIRBE's apertures are all there in concept, but their mathematical precision precludes optimum performance. That is, they are so closely lined up that even with first order theory there is not much of a break in the angle that the incoming ray diffracts to the next aperture. Hence, there is not as much attenuation, especially at the long wavelengths. This will be discussed in detail in Section 3.

In summary for this section, the DIRBE system has a tight constraint on its operating conditions, it is well designed for scattered light and has the making of an excellent system to suppress diffracted energy but isn't quite there yet. Based upon assumed mirror BRDFs, the performance will be limited by mirror scatter from the primary. Hence, the post launch scattering characteristics of the primary will be crucial.

3.0 SYSTEM MODEL

The DIRBE system is far more complex than is practical to fully model into APART. Most of the fine detail of nuts, bolts and rivets create no adverse impact on the final results when left out of the analysis. Every effort has been made to model the DIRBE system in sufficiently accurate detail in order to preclude erroneous results. The analysis was, in fact, delayed significantly because some APART program development was required before this analysis could be performed.

However, the system is modeled in detail from the Sunshield to the chopper blade. Many of the objects modeled into the analysis serve only an aesthetic purpose, having no impact on the system's performance. A profile of the system is shown in Figures 2, 4, 5 and 6 (at different profiles and scales). Note that the details of the vanes do not directly show up in the Figures. This is a characteristic of APART which considers the vanes as a complex absorbing coating.

The numbers shown in Figures 2, 4, 5, and 6 represent surfaces modeled into the program and the number by which this surface was designated in the analysis. In order to aid the reader, a literal assignment was also given to each object. The input file for Program 1 of APART is shown in Table 1A in Appendix A. This table calls out the object shape, number, and its assigned literal, along with additional program details.

3.1 Higher Levels Of Scatter

The program was modified to handle higher levels of propagation paths, i.e., it could trace more "bounces" of scatter, and/or more diffractions in a single path. The program arrays were increased in size in order to deal with nine (9) levels of scatter. For practical reasons, the program was not increased to the eleven levels of scatter or diffraction that are necessary for the very large off axis angles. The results for the larger off-axis angles, those that would require the 11 levels of scatter, have the final diffraction path going from the first field stop directly to the chopper. This will give results approximately three or four orders of magnitude above the expected diffraction results for the first three bands. There are several reasons that the higher level results were not pursued. In the lower three bands the diffraction is a relatively small contributor of power. The diffraction results, as calculated from FS1 directly to the chopper blades, push the computer limits on its exponential representation of numbers. The higher levels of diffraction would be treated as zeros. At the two longer wavebands (160um and 250um) the second field stop is so nearly aligned with the image of the first field stop (FS1) relative to the wavelength, that the PADE program automatically shifts from one type of diffraction analysis (STATIONARY Phase) to another (CONSTANT Phase) where there is very little attenuation due to the succeeding diffraction. In other words, the second field stop is ineffective.

Breault Research
Organization, Inc.

DIRBE X-Z PROFILE

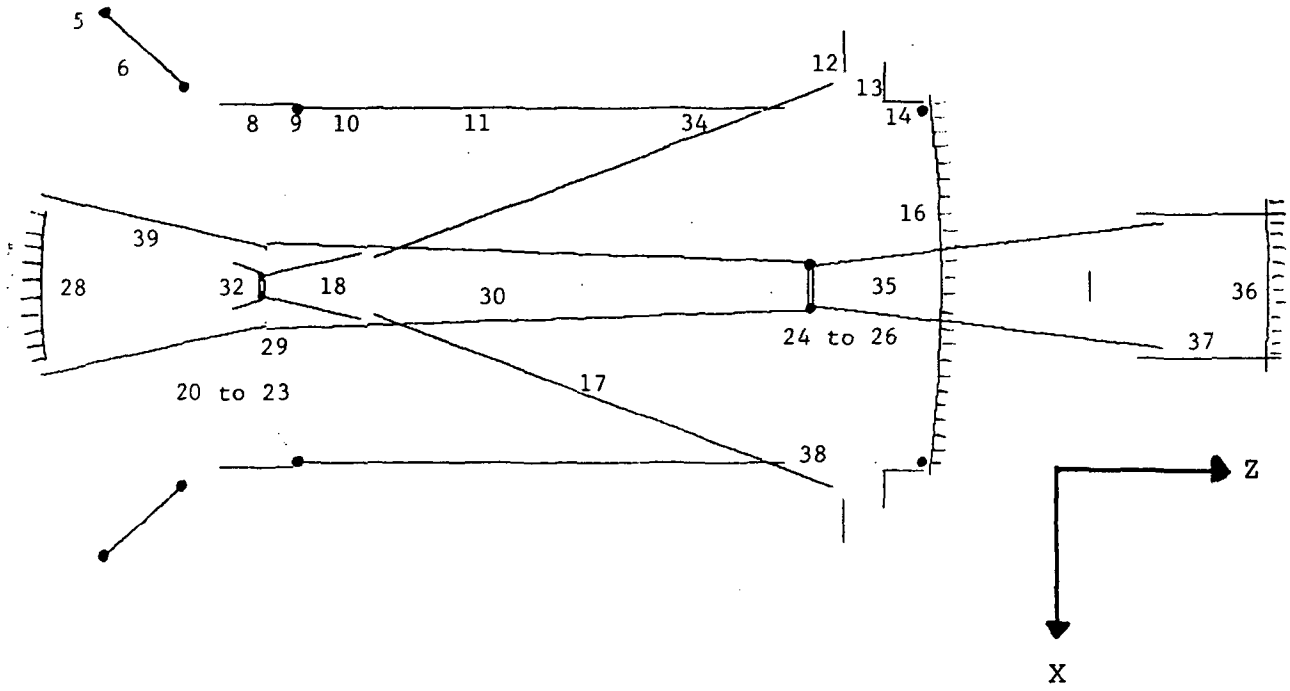

Figure 4. Profile X-Z plane DIRBE.

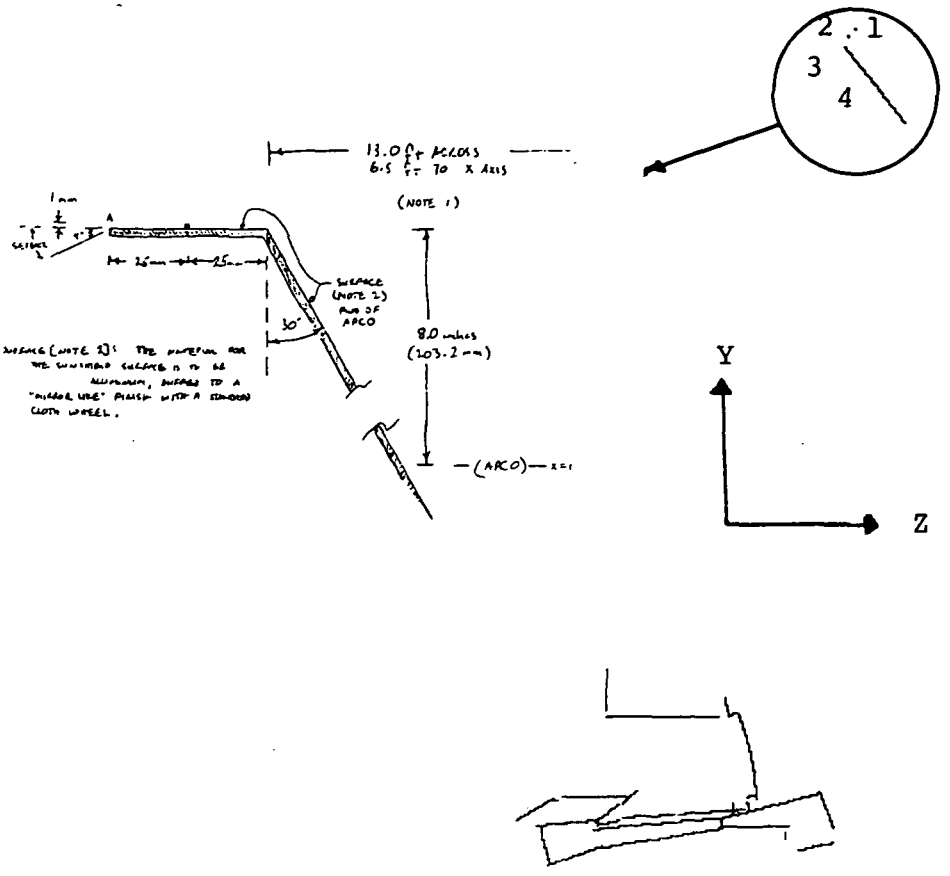

DIRBE Y-Z PROFILE

Figure 5. Profile Y-Z including sunshield.

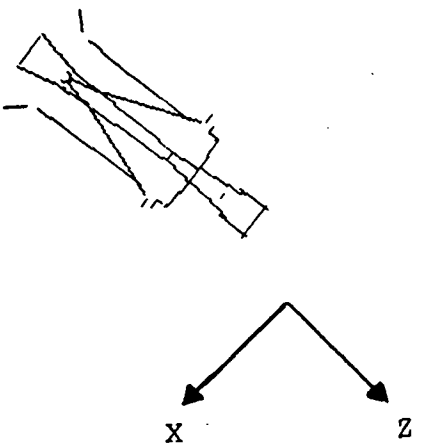

DIRBE X-Z PROFILE

Figure 6. Profile X-Z including sunshield.

The output will show the results of these complications in greater detail. In summary then, the predicted system performance will be accurate because mirror scatter dominates in the lower three bands and the diffraction from FS1 will closely approximate the system performance in the upper two bands where scatter is not as significant.

3.2 Sample Points For Diffraction

The shift from the more typical stationary phase contribution in the lower three bands to a constant phase contribution in the upper two bands required a more in depth analysis.

The APART/PADE program has two first order imaging routines that can be selected to calculate conjugate image locations. Both were used in the DIRBE analysis in order to try to determine the sensitivity of the diffraction from FS2 to the incoming diffracted energy from FS1. Nevertheless, both routines gave essentially the same results, indicating that the edges are optically very closely aligned.

An in depth analytical review revealed that the program was accurately calculating the performance based upon the finite set of points selected on each source and collector. Because of this mathematical sampling, there was a problem in the analysis that could be clearly explained but one that could not be restructured at this time. There is a set of conditions that are required for this problem to occur, and, unfortunately, all of them are satisfied for this portion of the analysis in DIRBE.

First, all the important source points, collector points, and diffraction peaks are in the meridional plane. Second, the diffraction peaks fall almost precisely on the sampled collector points. In the DIRBE analysis the source point is always in the meridional plane; only the 0 degree and 180 degree azimuths were analyzed. Second, all circular or elliptical diffracting edges had 6 sampling points. Hence, there always was a sample point in the 12 o'clock position and another one in the 6 o'clock position, see Figure 7. For the rectangular (square) apertures, the edges were made up of four straight edges with three sample points on each edge. For the top and bottom edges the center point was in the meridional plane, see Figure 8. By design FS1 is conjugate with FS2, thus satisfying the last condition.

Before jumping to any simple solutions, it is wrong to think that the solution is to move the sample points out of the meridional plane, which could easily have been done. Analytically the propagated energy would drop dramatically. Not only to a level well below those of this analysis, but also below the actual system performance. The reason is that for points in

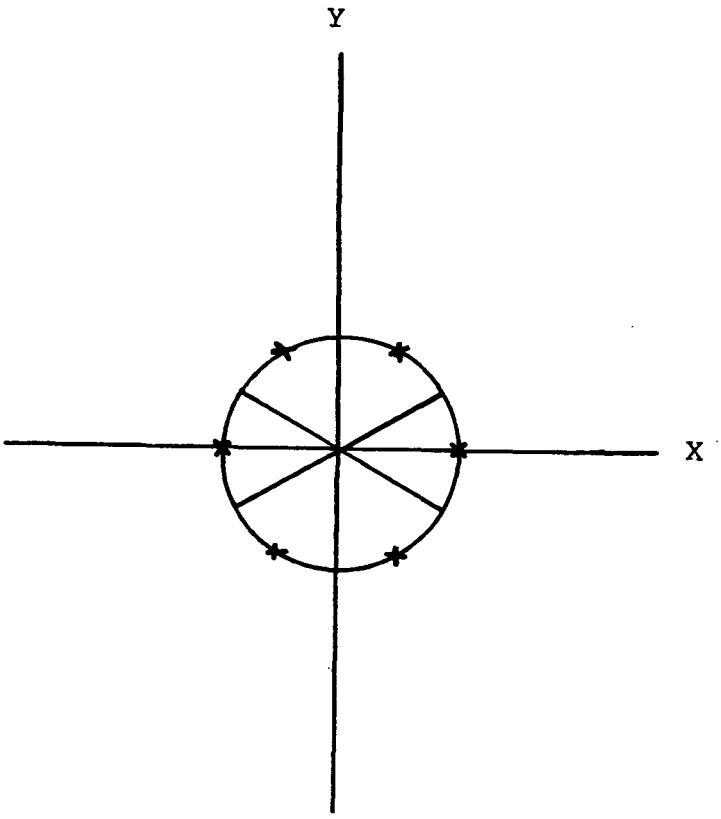

Figure 7. The X's mark the sampling points of the 6 pi sections used in the APART/PADE analysis.

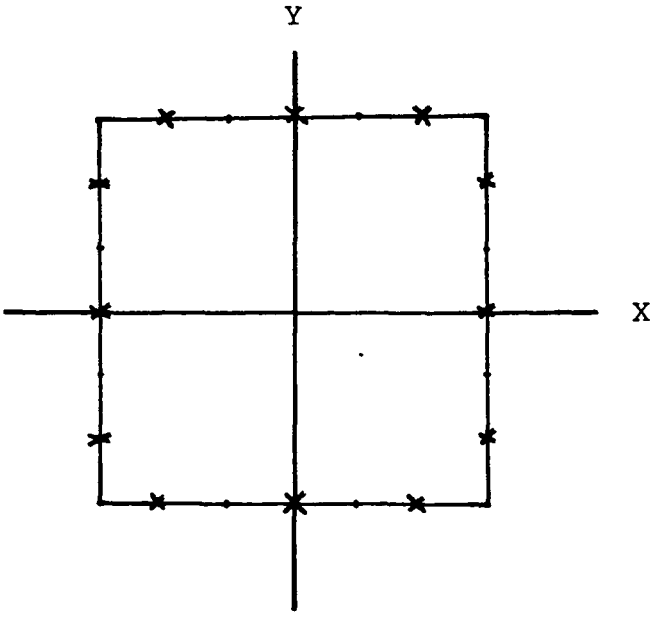

Figure 8. The X's mark the sampling points of the 3 sections of each diffracting edge.

the meridional plane, i.e., the ones used in this analysis, there is this nearly perfect alignment with a real peak (SPIKE) in the diffraction at the collector point as used in this analysis. That's all real and moving the collector point to some other location could give an apparently lower irradiance on the edge.

The real analytical problem is that the calculated values DO NOT represent the average values over the collector areas involved, i.e., the length of the following diffracting edges or the area on the chopper blade. The values accurately representing local peaks are "spread" over too large a source or collector areas, thereby calculating erroneously high propagated powers. Only super fine sampling could give sufficient resolution to resolve this kind of problem.

In the analysis this was not necessary because either the scatter from the primary mirror was the dominate source, or the diffraction from FS1 because of its alignment with FS2 dominated. When the diffraction from FS1 dominates, one of the major conditions above is not met. The FS1 and the chopper area are not conjugate. Therefore, the diffraction pattern is a relatively slow varying function, which means that the sampled points do represent the sampled area.

3.2.1 Aberrations -

There is one other limitation in the diffraction analysis. PADE stands for Paraxial Analysis of Diffracted Energy. There are optical aberrations in the real DIRBE system. The diffraction spikes discussed above were based on a first order, diffraction limited, type of system. In DIRBE the image of FS1, at FS2, is significantly aberrated. Because of these aberrations, some rays will get through FS2 and will then propagate to the edge of any image location, i.e., anything conjugate to the field stops. This will cause a local high around the edge of the image of the field stop. The same aberrated rays will be fairly uniformly spread over the Lyot stop, or any plane conjugate to it such as the chopper blade. The actual magnitude of this level of energy is dependent upon the optical design and its alignment. The solution is an optical design problem.

The quality of the image at the field stops can only be improved by using some of the parameters of the optical surfaces to improve the image quality, or by reducing the clear aperture size of the succeeding conjugate apertures in order to clip off all the aberrated rays. The latter is done in DIRBE to some extent.

When analyzing a system which is so closely aligned, the aberrations can also effect the calculated magnitude of the diffraction at the apertures. The actual irradiance could be higher or lower than the calculated values depending on the aberration, its sign, and its magnitude. The aberrations could move the centroid either closer to the edge or further away. In the analysis these aberrations play a role in the performance of the edges of

FS1 to FS2. Recall that the performance is limited by the primary and FS1, as presently designed. The near perfect alignment of FS1 and FS2 causes almost no change in the diffraction performance due to the second field stop.

3.2.2 Propagation Of Power -

The basic equation used in APART to trace the propagation of power is:

$$d\phi_c = L\, dA_s \cos\theta_s\, dA_c\, d\theta_c/R^2$$

The equation relating power transfer from one section to another is where $d\phi_c$ is the differential power transferred. L is the bidirectional radiance of the source section. dA_s and dA_c are the elemental areas of the source and collector. θ_s and θ_c are the angles that the line of sight from the source to the collector makes with their respective normals. This equation can be rewritten as three factors that help simplify the reduction of scattered radiation.

$$d\phi_c = \left(\frac{L}{E}\right)\left(dA_s E\right)\left(\frac{dA_c \cos\theta_c \cos\theta_s}{R^2}\right)$$

$$\phi_c = \text{BRDF}\ \phi_s\ \text{GCF}$$

where GCF stands for the Geometrical Configuration Factor, which is also the projected solid angle that the collector subtends from the source. An example is shown in Figure 9.

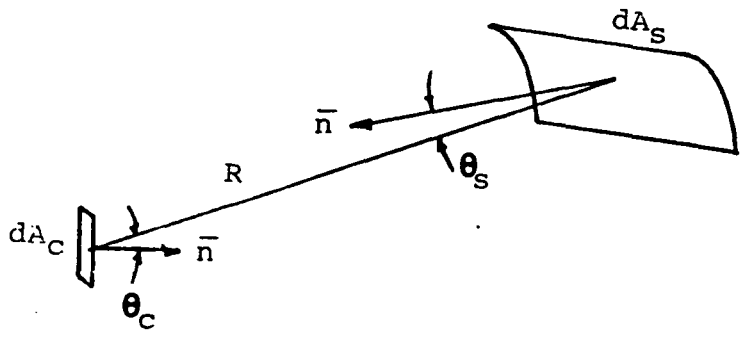

Figure 9. Example of the variables used in the above equation.

4.0 BRDF TERMINOLOGY

No measured data for the DIRBE optics exists. Therefore, the scattering characteristics of the mirrors had to be assumed. These characteristics are best presented in the form of a Bidirectional Reflectance Distribution Function (BRDF). In fact, the whole next section is dedicated to BRDFs. At first glance, it would seem that all bases are covered by the parametric analysis of the BRDF of the primary included in this report in the results section. Four different BRDFs were used to represent the different BRDFs that might be achieved for DIRBE's primary mirror; from excellent to less than average. That is all well and good for the first two, maybe three bands. What happens to the BRDFs out at 160 to 250 um is unknown. There is no BRDF data for mirror surfaces beyond 38 um. APART used a wavelength scaling law, that has a sound analytical basis, to scale the BRDFs from 10 um to 250 um, but there is no empirical data to corroborate such scaling.

Based upon the latest technology, it now seems possible to make such measurements. In the past, data has been presented that was thought to represent mirror BRDFs at long wavelengths. It is now understood that such data really represented the instrument profile, and not the BRDF of the mirror. The BRDF measurement of a mirror at the long wavelengths will be difficult because of the wavelength, the required detectors, and the very low BRDFs if the scaling law is accurate. There is some empirical support now that would indicate that nothing drastically changes the mirror BRDF's at the long wavelengths, as it does for black surfaces. The Infrared Astronomical Satellite (IRAS) had an operating range not too unlike DIRBE's. It did not show any startling changes in performance that could be attributed to the BRDFs of the mirrors.

4.1 BIDIRECTIONAL REFLECTANCE DISTRIBUTION FUNCTIONS (BRDF)

The absorbing and scattering characteristics of the surfaces in any system play a significant role in its ultimate stray light performance. The optical, baffle, and vane design play a more significant role because, unlike BRDFs, they can completely block a propagation path, i.e., make it go to zero, which is something no BRDF can achieve. DIRBE, by design, does all it can to block stray light paths. Those that are left are affected by the BRDFs of their surfaces.

In DIRBE we only have the following three (3) coatings to discuss:

1) Mirror BRDFs of the optical surfaces.

2) Blacks.

3) Mirror like finish of the forebaffle.

Diffraction is another type of "coating" that can be assigned to an edge since PADE allows the user to choose between Sommerfeld or Kirchhoff type diffraction.

In the DIRBE analysis, assumed BRDFs were used for the three more conventional coatings cited above.

The data are presented in a form called $\beta-\beta_0$ plot, after the Harvey-Shack theory. As shown in Figure 10, β_0 is the sine of the angle of specular reflection (even for a diffuse surface) and β is the sine of the observation angle. The data are then plotted on a log-log plot of the BRDF versus $\beta-\beta_0$. This type of plot is especially significant for micro rough surfaces, i.e. mirrors.

By design, there are so many light traps for sources beyond the plane of the sunshield that any reasonable variation in the BRDF of the forebaffle will probably not be significant. Its assumed BRDF is shown in Figure 11.

For the remaining paths of stray light, the BRDF of the black coating of the baffles on the main tube and the BRDF of the primary mirror are important and could result in DIRBE not meeting the required specs. The vanes were assumed to have Martin Black coating. Specific profiles of the APART BRDF models of Martin Black used for the analysis and some measured data are shown in Figures 12 and 13.

For the longer wavebands Martin Black turns specular, and as such is potentially a major problem. The program has a special specular vane cavity routine, developed for IRAS, that was used in this DIRBE analysis. This routine indicated that there were 24 specular paths from objects 6 to 11, then the primary and another 9 paths from 9 to 11, then to the primary. Fortunately, these affect only the higher off axis sources for which there is a sufficient margin of error.

The assumed BRDFs for the mirror in the 10.6 μm band are plotted in Figures 14 through 17 and are shown in Table 17. The data represents a range of BRDF's, any of which could be representative of a DIRBE primary. The BRDF's in the other bands were usually scaled from these values. The exceptions are shown in Figures 17 and 18 which are based on some actual measurements supplied by NASA (Appendix B).

We will present a BRDF scaling law that can be analytically derived, and which has been experimentally verified over small changes in wavelength. The data shown in Figures 17 and 18 for two different wavelengths on the same sample does not satisfy this scaling law. There are many reasons why this could happen. It could be simply that one or the other measurements are wrong. It could be that the physics of the scattering is different at the two wavelengths, i.e. one is particulate scatter, while the other is micro roughness scatter. The warning here is that the DIRBE mirrors should be measured - carefully - to determine their real BRDF. Furthermore, they,

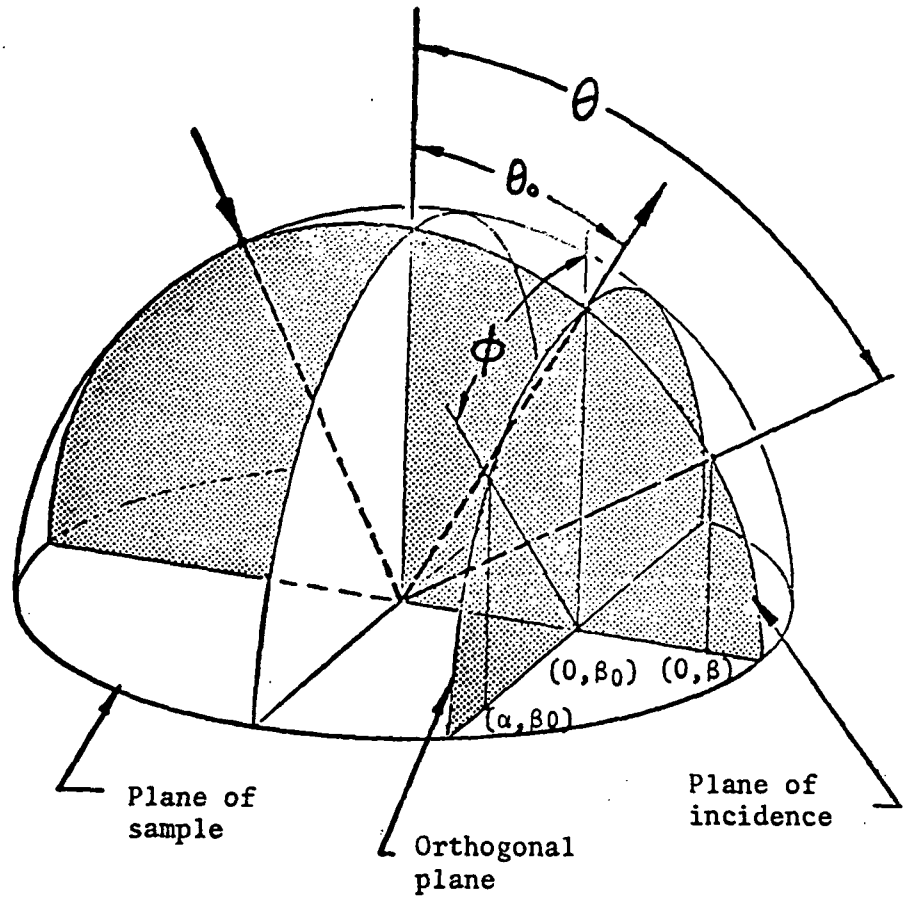

Figure 10. Pictorial representation of β and β_o which are used to plot BRDF data.

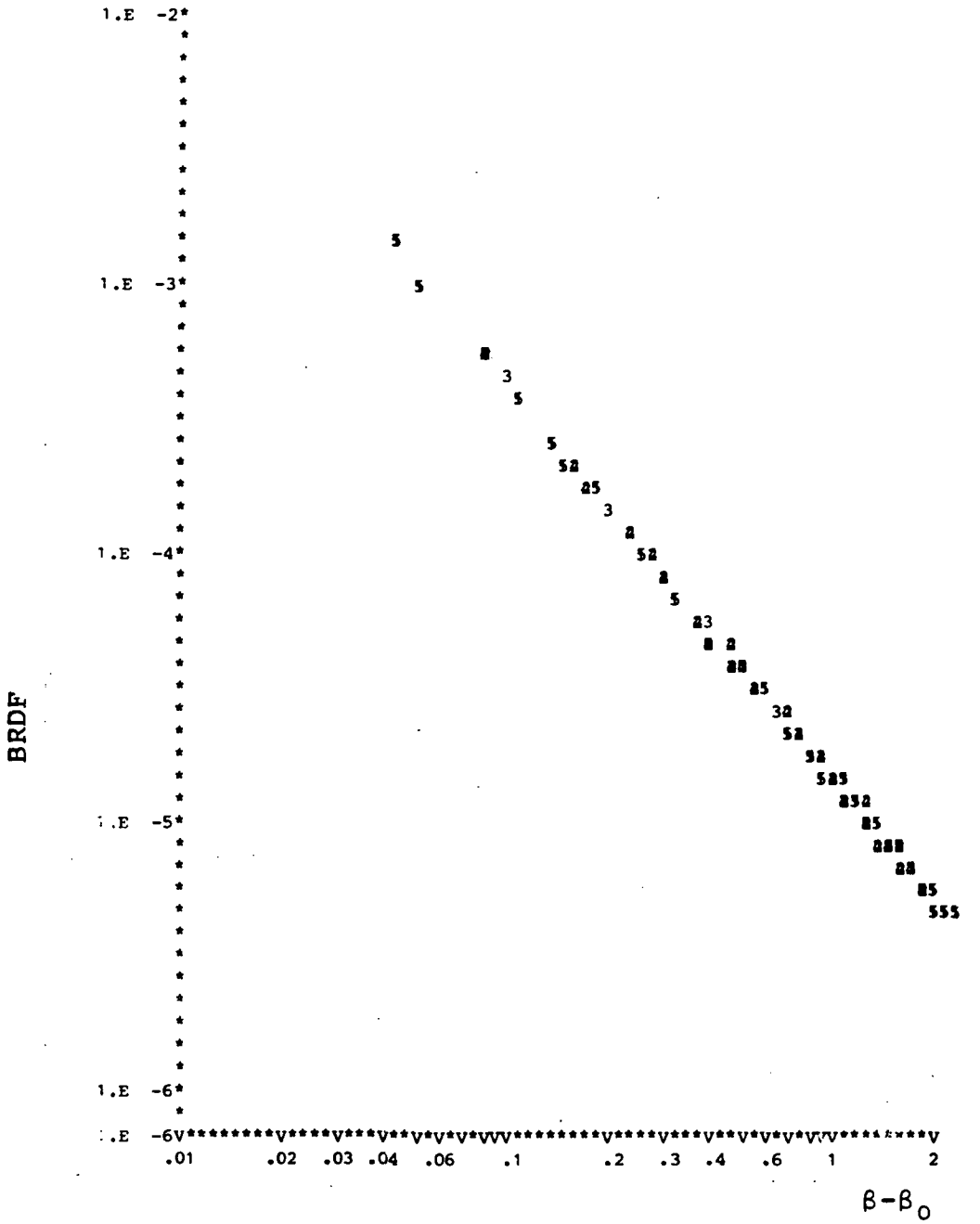

Figure 11. Mirror type BRDF of the foreshield.

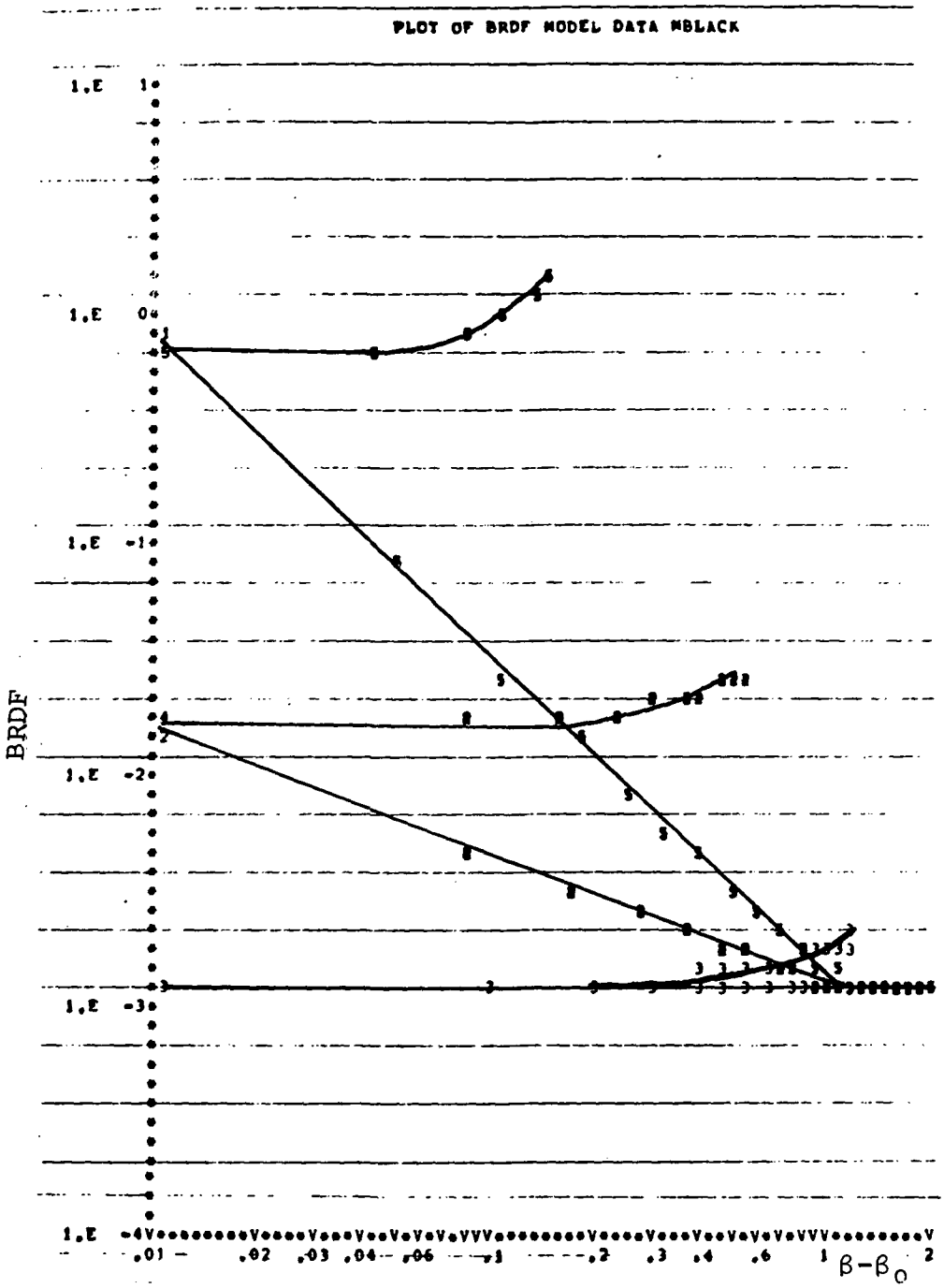

Figure 12. Measured Martin Black BRDF data.

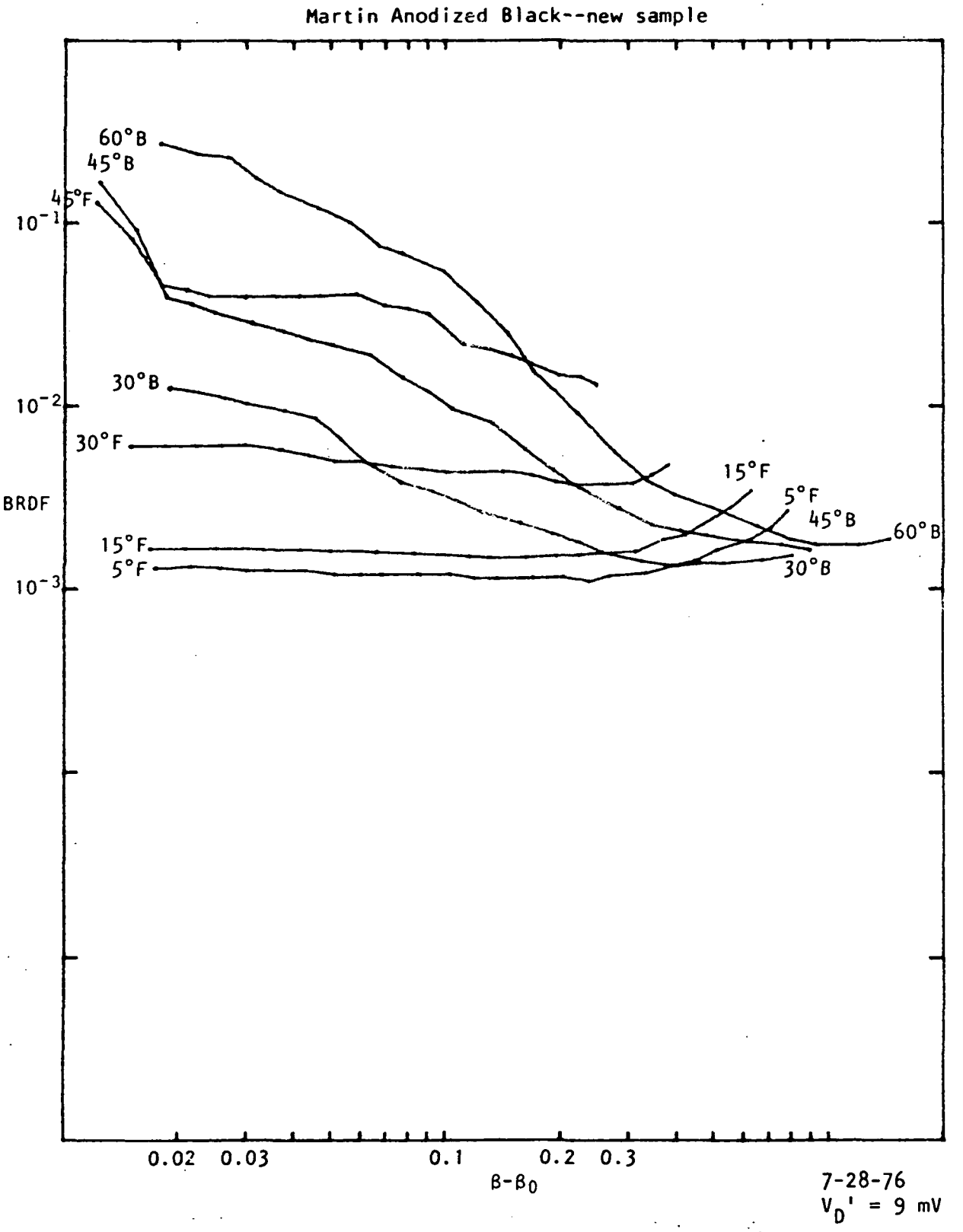

Figure 13. APART/PADE models of Martin Black at 10.6 μm.

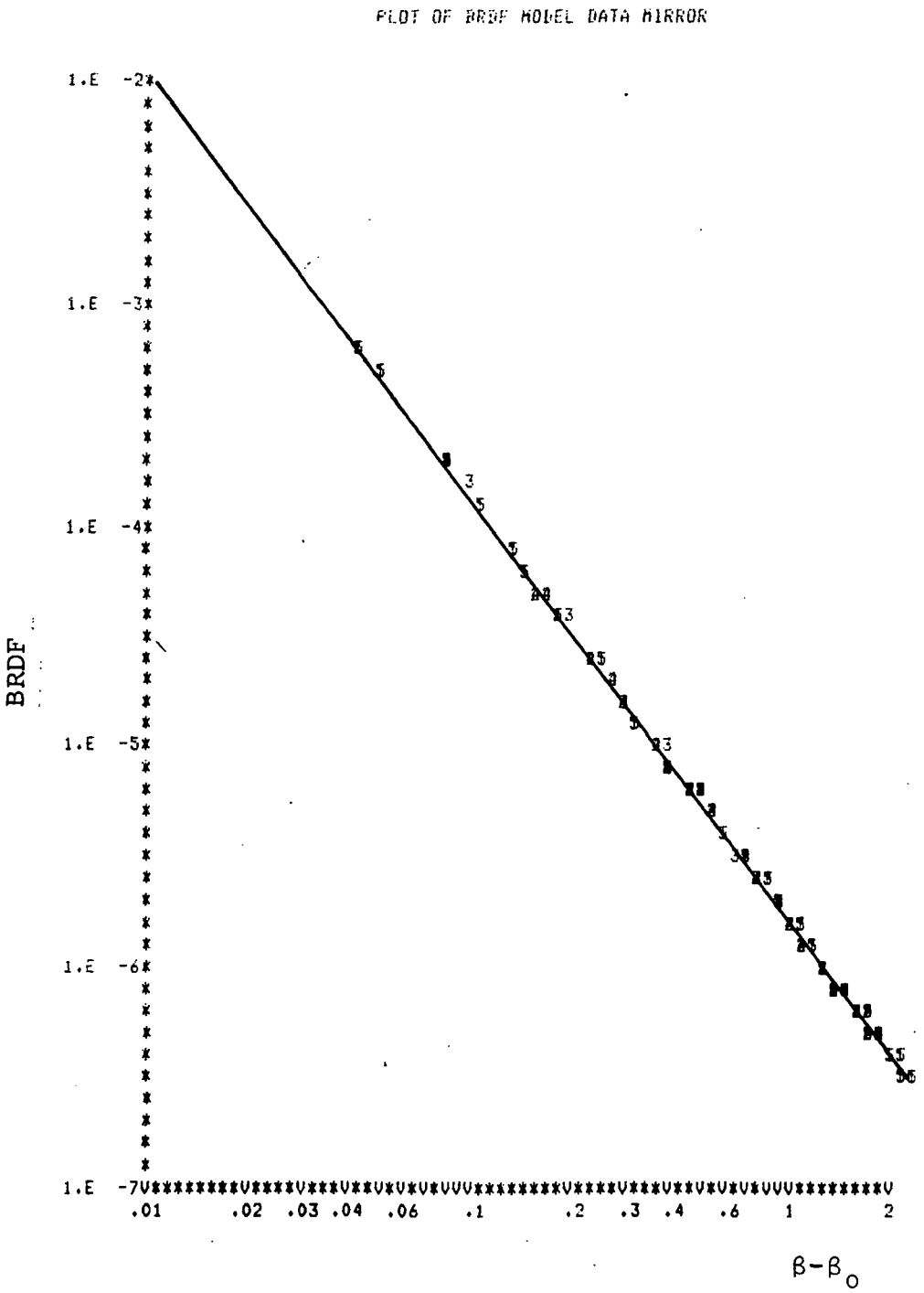

Figure 14. Nominal mirror BRDF.

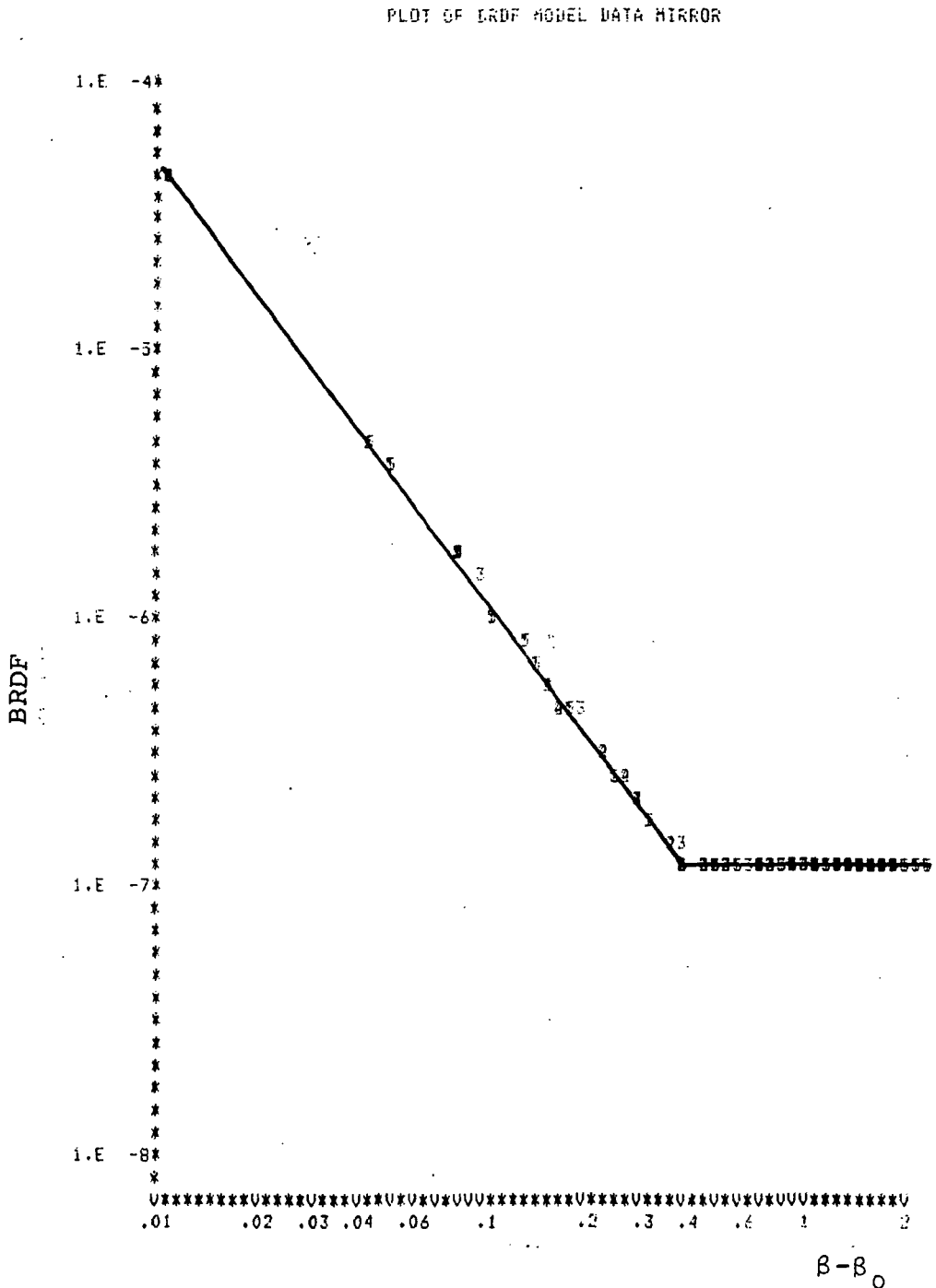

Figure 15. Mirror BRDF called the "Best" mirror in the analyses.

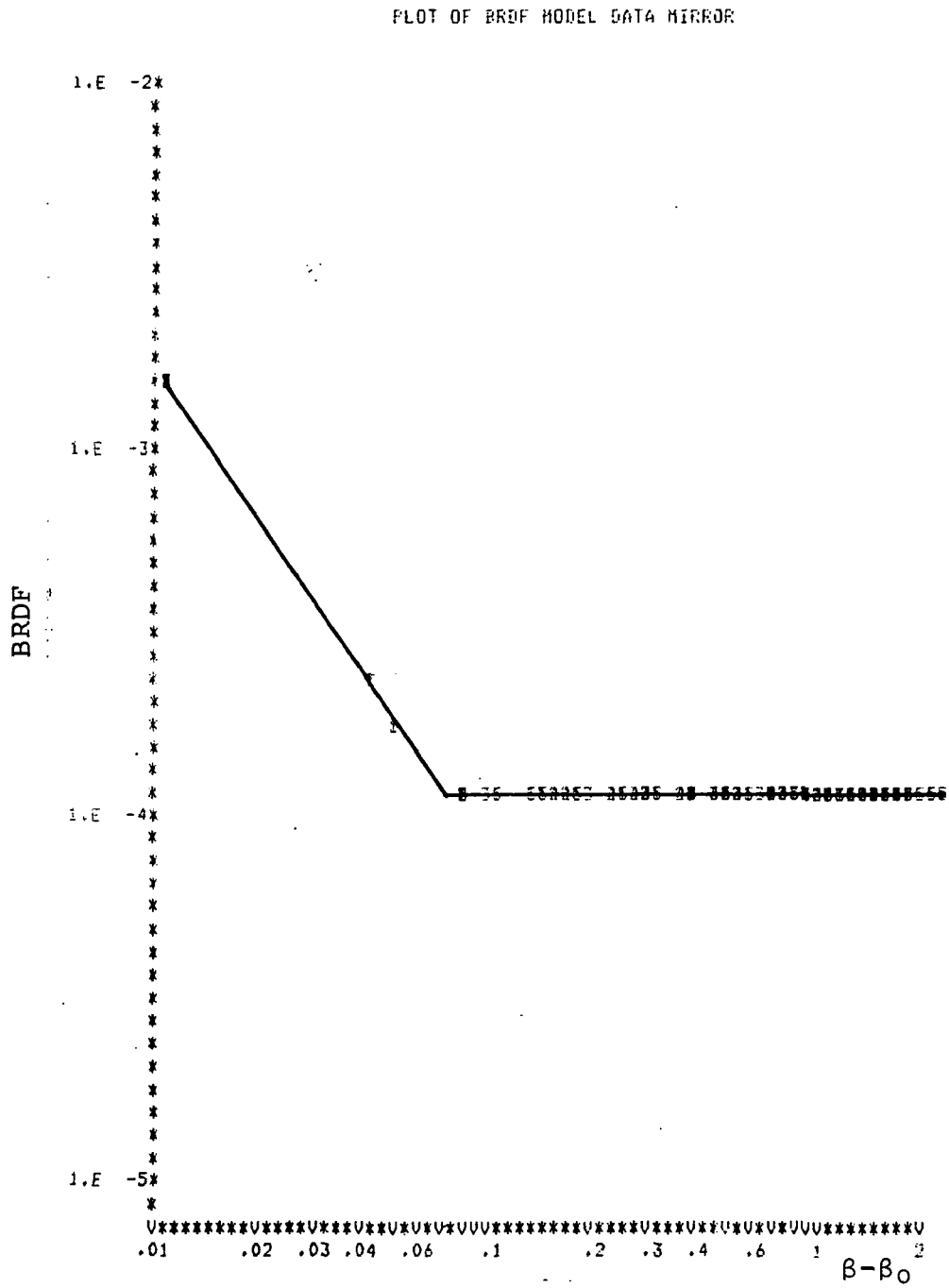

Figure 16. Mirror BRDF called the Diamond Turned mirror in the analyses.

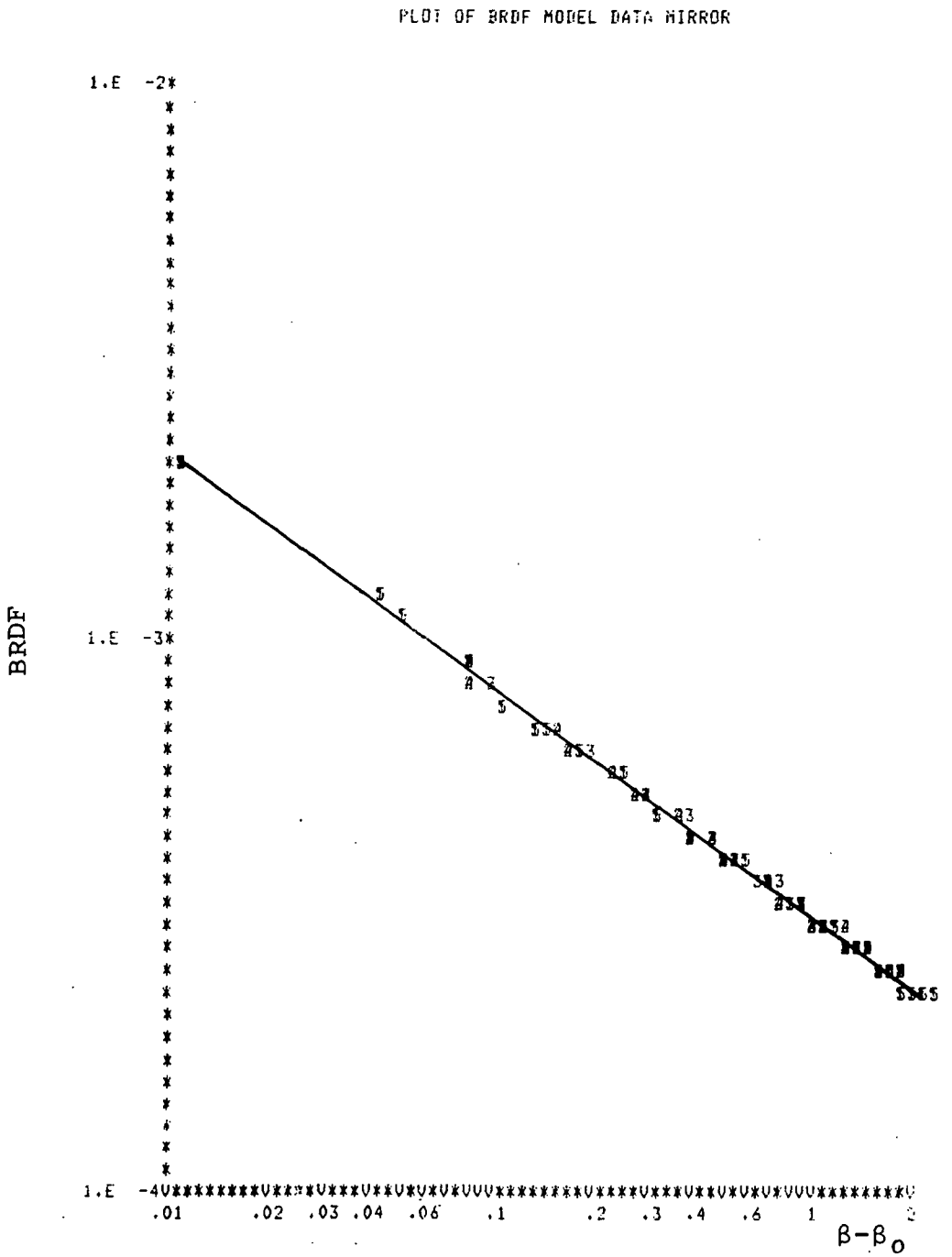

Figure 17. Mirror BRDF called the "Worst" mirror in the analyses at 10.6 μm.

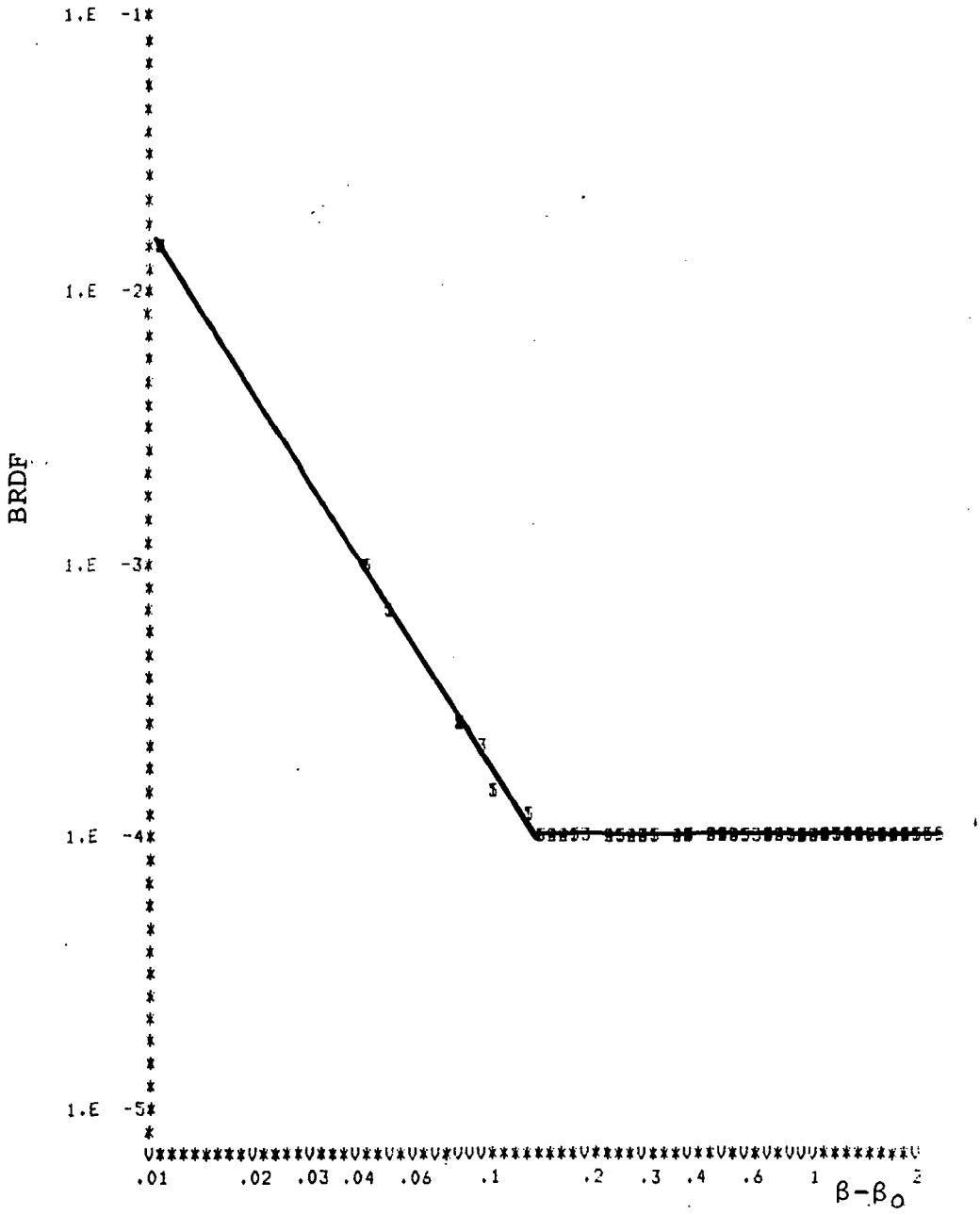

Figure 18. Mirror BRDF called the "Worst" mirror in the analyses at 1.25 μm.

or similar "witness" samples should be measured in several wavebands.

4.2 WAVELENGTH SCALING LAW

Based on Harvey's work, the BRDF of a micro rough surface can be scaled from one wavelength to another; at least over short changes in wavelength. The Harvey wavelength scaling law is:

$$S(\alpha,\beta,a\lambda) = \frac{1}{a^4} S\left(\frac{\alpha}{a},\frac{\beta}{a};\lambda\right)$$

This equation reflects a change in the amplitude of scatter and in the direction of the scattered radiation because of the change in wavelength. The formulation is closely tied to diffraction from a diffraction grating.

This equation can be reworked to a more meaningful one for APART data input. In APART a BRDF for a mirror is put in as a starting value and a slope. Therefore, the APART scaling law is

$$S(\beta-\beta_0 = .01\ a\lambda) = a^{-(4+s)}\ S(\beta-\beta_0 = .01;\lambda)$$

where s is the slope of the line of the BRDF in log ($\beta - \beta_0$) versus log (BRDF).

5.0 RESULTS

The stray light analysis is best broken down into meaningful sets of separate analyses. The two major tasks involved the response of the system to a point source, first in the zero degree azimuth, then in the 180 degree azimuthal direction. The off-axis angles, relative to the optical axis of the instrument were 5, 20, 40, 64, 100, 124, 130, and 150 degrees. These angles are not relative to the spin axis which was 30 degrees from the optical axis in the 180 degree azimuth. Therefore, the 124 degree position

represents 94 degrees from the spin axis in the 180 degree azimuth. Likewise, the 64 degree position represents 94 degrees from the spin axis in the zero degree azimuth. Hence, the range of angles covers point sources that are sufficiently near the field of view so as to put power directly on the primary, to angles just beyond the sunshield, and slightly beyond.

The most significant propagation paths will vary as the point source moves further, and further from the optical axis. But the analysis showed that the last portion of the paths remained the same for all angles, and all wavelengths. The scatter off the primary mirror to the chopper, and the diffraction from the field stops to the chopper were the major final paths of the propagated energy. Table 3 is an example of one such path. Table 3A in Appendix A has the full input for the analysis, hence each path is listed in detail there. In Table 3 the first row has only the point source object number (99). The second row contains objects (by number as used in APART, see Figure 3) that the point source energy can reach directly. In the example it is object 1, the outer diffracting edge of the sunshield. The next row contains the collector(s) for object 1, in this case only object 2. Three and four are collectors for object two, while 5 and 6 collect diffracted power from edge 3. The method continues until object 16 scatters to 98 the detector, while the diffracted energy is still propagating to the first Field Stop (FS1). From there the diffracted energy eventually reaches the chopper (98). The program keeps all these paths separated and tallies the results in the form of Percent Tables, as shown in the many Tables in this section.

Table 3. Propagation Paths for Large Off-axis Angles.

PATHS
99
1
2
3 4
5 6
10 11
15 16
20 21 22 23 98
98

The APART output gives Percent Tables as a function of the scattering "level", Table 4, or as a function of the position of the point source. The latter condenses each of the former Tables into one column. For example, the data in Table 4, is condensed into the first column of the data in Table 5.

Table 4 PERCENT OF POWER CONTRIBUTED BY EACH OBJECT AS A FUNCTION OF EACH SCATTERING LEVEL

OFF AXIS POSITION 1 5.000 DEGREES 180.000 AZIMUTH

OBJECTS/	LEVEL OF SCATTER				
	1	2	3	4	5
16 PRI MIR	0.00	100.00	0.00	0.00	0.00
24 TOP F2	0.00	0.00	0.00	0.00	92.20
25 RT F2	0.00	0.00	0.00	0.00	0.05
26 BOT F2	0.00	0.00	0.00	0.00	7.71
27 LEF F2	0.00	0.00	0.00	0.00	0.05
TOTAL POWER	0.00E+00	6.35E-02	0.00E+00	0.00E+00	7.17E-13

Table 5 BAND 1 180 DEGREES AZIMUTH
PERCENT OF POWER CONTRIBUTED
BY EACH OBJECT AS A FUNCTION
OF OFF AXIS SOURCE POSITION

OBJECTS/	OFF AXIS POSITION							
	1	2	3	4	5	6	7	8
16 PRI MIR	100.00	100.00	100.00	100.00	100.00	100.00	100.00	100.00
20 TOP F1	0.00	0.00	0.00	0.00	0.00	0.00	0.00	0.00
21 RT F1	0.00	0.00	0.00	0.00	0.00	0.00	0.00	0.00
22 BOT F1	0.00	0.00	0.00	0.00	0.00	0.00	0.00	0.00
23 LEF F1	0.00	0.00	0.00	0.00	0.00	0.00	0.00	0.00
24 TOP F2	0.00	0.00	0.00	0.00	0.00	0.00	0.00	0.00
25 RT F2	0.00	0.00	0.00	0.00	0.00	0.00	0.00	0.00
26 BOT F2	0.00	0.00	0.00	0.00	0.00	0.00	0.00	0.00
27 LEF F2	0.00	0.00	0.00	0.00	0.00	0.00	0.00	0.00
TOTAL POWER	6.35E-02	7.13E-04	4.19E-08	1.88E-08	2.83E-09	3.37E-27	7.44E-29	5.94E-30
SOURCE ANG	5.0	20.0	40.0	64.0	100.0	124.0	130.0	150.0

In a poorly baffled system the Percent Tables that give the power as a function of the scattering level can help to unravel the paths involved. In Dirbe the allowed propagation paths are controlled and understood. Therefore, the Percent Tables as a function of the point source are the only ones presented. There are plenty of those alone.

APART also gives the power distribution at the different sample points for each collector. It is of interest to note that the power distribution for DIRBE at the chopper will be relatively uniform. Representative data is shown in Table 6. This type of distribution is due to the optical design. The Critical objects that are the main contributors to the chopper are either uniformly illuminated or are far from the collector, sufficiently so that the difference in the flux density in their wavefront is small.

Table 6 OBJECT 98 THE IMAGE CHOP
THE POWER DISTRIBUTION ON OBJECT 98

1	9.08E-14	9.08E-14	9.08E-14
2	1.36E-13	1.04E-13	1.36E-13
3	2.28E-14	2.28E-14	2.28E-14

There were five different wavebands that were analyzed, as shown in Table 1. For each azimuth there will be a percent Table showing the systems performance as a function of the position of the point source. The paths were the same in each case, only the BRDFs were changed when going from one waveband to the next. The results for the 180 degree azimuth (+Y in Figure 3) are presented in Tables 5, 7, 8, 9, and 10, for each waveband.

Table 7 BAND 2 180 DEGREES AZIMUTH
PERCENT OF POWER CONTRIBUTED
BY EACH OBJECT AS A FUNCTION
OF OFF AXIS SOURCE POSITION

OBJECTS/	OFF AXIS POSITION							
	1	2	3	4	5	6	7	8
16 PRI MIR	98.97	98.26	99.91	99.92	100.00	96.63	96.48	91.98
20 TOP F1	0.91	1.60	0.00	0.00	0.00	0.21	0.33	3.91
21 RT F1	0.00	0.00	0.00	0.00	0.00	0.40	0.41	0.82
22 BOT F1	0.13	0.14	0.00	0.00	0.00	2.36	2.38	2.49
23 LEF F1	0.00	0.00	0.00	0.00	0.00	0.39	0.41	0.80
24 TOP F2	0.00	0.00	0.09	0.08	0.00	0.00	0.00	0.00
25 RT F2	0.00	0.00	0.00	0.00	0.00	0.00	0.00	0.00
26 BOT F2	0.00	0.00	0.00	0.00	0.00	0.00	0.00	0.00
27 LEF F2	0.00	0.00	0.00	0.00	0.00	0.00	0.00	0.00
TOTAL POWER	8.92E-04	1.01E-05	3.37E-09	8.60E-10	3.93E-11	1.49E-28	3.38E-30	9.12E-31
SOURCE ANG	5.0	20.0	40.0	64.0	100.0	124.0	130.0	150.0

Table 8 BAND 3 180 DEGREES AZIMUTH
PERCENT OF POWER CONTRIBUTED
BY EACH OBJECT AS A FUNCTION
OF OFF AXIS SOURCE POSITION

OBJECTS/	OFF AXIS POSITION							
	1	2	3	4	5	6	7	8
16 PRI MIR	99.32	98.86	59.77	61.26	99.98	21.17	12.67	6.02
20 TOP F1	0.00	0.00	0.00	0.00	0.00	4.74	25.37	44.89
21 RT F1	0.00	0.00	0.00	0.00	0.00	3.24	6.78	10.36
22 BOT F1	0.00	0.00	0.00	0.00	0.00	67.63	48.54	28.64
23 LEF F1	0.00	0.00	0.00	0.00	0.00	3.23	6.64	10.10
24 TOP F2	0.63	1.08	38.44	36.77	0.00	0.00	0.00	0.00
25 RT F2	0.00	0.01	0.31	0.31	0.00	0.00	0.00	0.00
26 BOT F2	0.05	0.05	1.15	1.36	0.01	0.00	0.00	0.00
27 LEF F2	0.00	0.01	0.32	0.31	0.00	0.00	0.00	0.00
TOTAL POWER	6.92E-05	7.80E-07	1.50E-09	3.32E-10	3.06E-12	5.68E-28	2.84E-29	1.28E-28
SOURCE ANG	5.0	20.0	40.0	64.0	100.0	124.0	130.0	150.0

Table 9 BAND 4 180 DEGREES AZIMUTH
PERCENT OF POWER CONTRIBUTED
BY EACH OBJECT AS A FUNCTION
OF OFF AXIS SOURCE POSITION

OBJECTS/	OFF AXIS POSITION							
	1	2	3	4	5	6	7	8
16 PRI MIR	4.18	2.50	0.33	0.33	60.98	0.50	0.29	0.06
20 TOP F1	0.00	0.00	0.00	0.00	0.00	8.10	13.93	22.57
21 RT F1	0.00	0.00	0.00	0.00	0.00	4.16	7.89	13.82
22 BOT F1	0.00	0.00	0.00	0.00	0.00	83.08	70.14	50.07
23 LEF F1	0.00	0.00	0.00	0.00	0.00	4.15	7.74	13.48
24 TOP F2	86.82	91.15	80.91	77.28	3.06	0.00	0.00	0.00
25 RT F2	0.39	0.38	0.87	0.87	0.34	0.00	0.00	0.00
26 BOT F2	8.23	5.59	17.03	20.66	35.28	0.00	0.00	0.00
27 LEF F2	0.39	0.38	0.87	0.87	0.34	0.00	0.00	0.00
TOTAL POWER	9.26E-05	1.74E-06	6.35E-08	1.38E-08	2.83E-13	3.73E-24	1.55E-25	5.55E-25
SOURCE ANG	5.0	20.0	40.0	64.0	100.0	124.0	130.0	150.0

Table 10 BAND 5 180 DEGREES AZIMUTH
PERCENT OF POWER CONTRIBUTED
BY EACH OBJECT AS A FUNCTION
OF OFF AXIS SOURCE POSITION

OBJECTS/	OFF AXIS POSITION							
	1	2	3	4	5	6	7	8
16 PRI MIR	0.89	0.53	0.08	0.08	22.88	0.20	0.11	0.02
20 TOP F1	0.00	0.00	0.00	0.00	0.00	8.55	11.30	14.98
21 RT F1	0.00	0.00	0.00	0.00	0.00	5.12	10.82	18.62
22 BOT F1	0.00	0.00	0.00	0.00	0.00	81.03	67.16	48.22
23 LEF F1	0.00	0.00	0.00	0.00	0.00	5.10	10.61	18.15
24 TOP F2	89.02	92.24	73.91	69.25	5.39	0.00	0.00	0.00
25 RT F2	0.61	0.59	0.95	0.95	1.25	0.00	0.00	0.00
26 BOT F2	8.87	6.05	24.11	28.77	69.23	0.00	0.00	0.00
27 LEF F2	0.61	0.59	0.95	0.95	1.25	0.00	0.00	0.00
TOTAL POWER	1.78E-04	3.35E-06	1.60E-07	3.53E-08	3.09E-13	2.17E-23	1.46E-24	5.69E-24
SOURCE ANG	5.0	20.0	40.0	64.0	100.0	124.0	130.0	150.0

The following five sets of data are for the 5 wavebands with the point source in the zero degree azimuth (the -Y direction as shown in Figure 3).

Table 11 BAND 1 ZERO DEGREES AZIMUTH
PERCENT OF POWER CONTRIBUTED
BY EACH OBJECT AS A FUNCTION
OF OFF AXIS SOURCE POSITION

OBJECTS/	OFF AXIS POSITION							
	1	2	3	4	5	6	7	8
16 PRI MIR	100.00	100.00	100.00	100.00	100.00	100.00	100.00	100.00
20 TOP F1	0.00	0.00	0.00	0.00	0.00	0.00	0.00	0.00
21 RT F1	0.00	0.00	0.00	0.00	0.00	0.00	0.00	0.00
22 BOT F1	0.00	0.00	0.00	0.00	0.00	0.00	0.00	0.00
23 LEF F1	0.00	0.00	0.00	0.00	0.00	0.00	0.00	0.00
24 TOP F2	0.00	0.00	0.00	0.00	0.00	0.00	0.00	0.00
25 RT F2	0.00	0.00	0.00	0.00	0.00	0.00	0.00	0.00
26 BOT F2	0.00	0.00	0.00	0.00	0.00	0.00	0.00	0.00
27 LEF F2	0.00	0.00	0.00	0.00	0.00	0.00	0.00	0.00
TOTAL POWER	7.11E-02	6.96E-04	1.14E-08	3.35E-27	4.09E-30	3.33E-30	3.29E-30	3.20E-30
SOURCE ANG	5.0	20.0	40.0	64.0	100.0	124.0	130.0	150.0

Table 12 BAND 2 ZERO DEGREES AZIMUTH
PERCENT OF POWER CONTRIBUTED
BY EACH OBJECT AS A FUNCTION
OF OFF AXIS SOURCE POSITION

OBJECTS/	OFF AXIS POSITION							
	1	2	3	4	5	6	7	8
16 PRI MIR	100.00	100.00	99.98	90.53	90.81	91.48	91.63	91.84
20 TOP F1	0.00	0.00	0.00	0.60	0.65	0.93	1.07	1.79
21 RT F1	0.00	0.00	0.00	0.01	0.04	0.14	0.18	0.34
22 BOT F1	0.00	0.00	0.00	8.85	8.45	7.31	6.96	5.69
23 LEF F1	0.00	0.00	0.00	0.01	0.04	0.13	0.17	0.33
24 TOP F2	0.00	0.00	0.00	0.00	0.00	0.00	0.00	0.00
25 RT F2	0.00	0.00	0.00	0.00	0.00	0.00	0.00	0.00
26 BOT F2	0.00	0.00	0.02	0.00	0.00	0.00	0.00	0.00
27 LEF F2	0.00	0.00	0.00	0.00	0.00	0.00	0.00	0.00
TOTAL POWER	9.88E-04	9.69E-06	9.56E-10	2.66E-26	2.01E-29	7.53E-30	6.28E-30	3.77E-30
SOURCE ANG	5.0	20.0	40.0	64.0	100.0	124.0	130.0	150.0

Table 13 BAND 3 ZERO DEGREES AZIMUTH
PERCENT OF POWER CONTRIBUTED
BY EACH OBJECT AS A FUNCTION
OF OFF AXIS SOURCE POSITION

OBJECTS/	OFF AXIS POSITION							
	1	2	3	4	5	6	7	8
16 PRI MIR	99.68	99.43	88.09	6.70	6.92	7.51	7.66	7.96
20 TOP F1	0.00	0.00	0.00	5.60	6.00	8.49	9.79	17.01
21 RT F1	0.00	0.00	0.00	0.07	0.32	1.33	1.75	3.69
22 BOT F1	0.00	0.00	0.00	87.57	86.46	81.38	79.10	67.75
23 LEF F1	0.00	0.00	0.00	0.06	0.31	1.29	1.70	3.59
24 TOP F2	0.04	0.05	0.78	0.00	0.00	0.00	0.00	0.00
25 RT F2	0.00	0.00	0.06	0.00	0.00	0.00	0.00	0.00
26 BOT F2	0.27	0.51	11.01	0.00	0.00	0.00	0.00	0.00
27 LEF F2	0.00	0.00	0.06	0.00	0.00	0.00	0.00	0.00
TOTAL POWER	8.59E-05	8.44E-07	3.07E-10	4.13E-24	3.01E-27	1.04E-27	8.46E-28	4.83E-28
SOURCE ANG	5.0	20.0	40.0	64.0	100.0	124.0	130.0	150.0

Table 14 BAND 4 ZERO DEGREES AZIMUTH
PERCENT OF POWER CONTRIBUTED
BY EACH OBJECT AS A FUNCTION
OF OFF AXIS SOURCE POSITION

OBJECTS/	OFF AXIS POSITION							
	1	2	3	4	5	6	7	8
16 PRI MIR	5.82	3.27	0.20	0.04	0.04	0.05	0.05	0.06
20 TOP F1	0.00	0.00	0.00	7.22	7.30	7.85	8.16	10.10
21 RT F1	0.00	0.00	0.00	0.14	0.36	1.25	1.64	3.60
22 BOT F1	0.00	0.00	0.00	92.47	91.96	89.64	88.56	82.75
23 LEF F1	0.00	0.00	0.00	0.13	0.34	1.21	1.59	3.50
24 TOP F2	11.07	7.65	5.86	0.00	0.00	0.00	0.00	0.00
25 RT F2	0.41	0.41	0.62	0.00	0.00	0.00	0.00	0.00
26 BOT F2	82.29	88.26	92.70	0.00	0.00	0.00	0.00	0.00
27 LEF F2	0.41	0.41	0.62	0.00	0.00	0.00	0.00	0.00
TOTAL POWER	7.45E-05	1.30E-06	3.07E-08	4.05E-20	2.95E-23	9.82E-24	7.88E-24	4.12E-24
SOURCE ANG	5.0	20.0	40.0	64.0	100.0	124.0	130.0	150.0

Table 15 BAND 5 ZERO DEGREES AZIMUTH
PERCENT OF POWER CONTRIBUTED
BY EACH OBJECT AS A FUNCTION
OF OFF AXIS SOURCE POSITION

OBJECTS/	OFF AXIS POSITION							
	1	2	3	4	5	6	7	8
16 PRI MIR	1.18	0.66	0.04	0.01	0.01	0.02	0.02	0.02
20 TOP F1	0.00	0.00	0.00	7.36	7.38	7.62	7.77	8.72
21 RT F1	0.00	0.00	0.00	0.21	0.51	1.75	2.28	4.96
22 BOT F1	0.00	0.00	0.00	92.24	91.61	88.93	87.74	81.48
23 LEF F1	0.00	0.00	0.00	0.18	0.48	1.69	2.20	4.82
24 TOP F2	10.50	7.18	5.19	0.00	0.00	0.00	0.00	0.00
25 RT F2	0.62	0.60	0.73	0.00	0.00	0.00	0.00	0.00
26 BOT F2	87.08	90.97	93.31	0.00	0.00	0.00	0.00	0.00
27 LEF F2	0.62	0.60	0.73	0.00	0.00	0.00	0.00	0.00
TOTAL POWER	1.50E-04	2.66E-06	1.09E-07	2.56E-19	2.93E-22	9.77E-23	7.86E-23	4.14E-23
SOURCE ANG	5.0	20.0	40.0	64.0	100.0	124.0	130.0	150.0

Table 16 shows the power due to internal thermally emitted radiation. There is no data for Band 1 because the values are so low they were beyond the normal exponential limit used in the computer.

Table 16 THERMAL
INPUT DECK IS CALLED DIRTHR
SEP 11 1983
-STRAYLIGHT ANALYSIS
- NOMINAL DESIGN
THERMAL EMISSION ANALYSIS

PERCENT OF POWER CONTRIBUTED
BY EACH OBJECT AS A FUNCTION
OF OFF AXIS SOURCE POSITION

OBJECTS/	OFF AXIS POSITION			
	1	2	3	4
16 PRI MIR	100.00	95.98	11.96	4.01
24 TOP F2	0.00	3.18	42.23	35.35
25 RT F2	0.00	0.21	8.62	13.85
26 BOT F2	0.00	0.42	28.65	32.99
27 LEF F2	0.00	0.21	8.54	13.80
TOTAL POWER	2.10E-24	6.44E-28	5.47E-27	2.36E-27
	BAND 2	BAND 3	BAND 4	BAND 5

The 5 BRDFs used in the parametric analysis of the primary mirror's contribution of stray light to the detector are shown in Table 17 and are taken from the data presented in Figure C1 (Appendix B).

Table 17. Primary Mirror BRDFs.

	BRDF ($\beta-\beta_o$ = .01)	Slope	Min. BRDF	
1 Standard Al on Fused Silica Basic Analysis (Tables 5, 7, 8, 9, 10, 11, 12, 13, 14, 15, and 16)	.01	-2	1.E-8	10.6
2 Vapor deposited Al on super polished Kanigen Best Mirror (Table 18)	.00004	-1.66	1.E-7	10.6
3 Worst (Dusty) Mirror (Table 19)	.0133	-1.97	1.E-4	1.25
	.002	- .43	1.E-4	10.6
4 Vapor deposited Al on diamond turned mirror Diamond Turned (Table 20)	.01	-1.42	1.E-4	10.6

Table 18 is one part of a parametric analysis of the affects of the BRDF of the primary mirror. The table is a composite of 5 separate runs that analyzed ONLY the contribution from the primary mirror. That is why the composite percent table shows that 100% of the power is coming from the primary. The data is to be compared to the power contributed by the primary as shown in Tables 5, 7, 8, 9, and 10 (Bands 1, 2, 3, 4, and 5, also at 180 degrees). However, the assigned BRDF to the primary is the best (lowest) of the BRDFs supplied by NASA (Appendix B) (#2 in Table 17).

Table 18 180 DEGREES AZIMUTH BEST MIRROR PERCENT OF POWER CONTRIBUTED BY EACH OBJECT AS A FUNCTION OF OFF AXIS SOURCE POSITION

OBJECTS/	OFF AXIS POSITION							
	1	2	3	4	5	6	7	8
16 PRI MIR	100.00	100.00	100.00	100.00	100.00	100.00	100.00	100.00
BAND 1 POWER	1.10E-03	1.97E-05	5.68E-10	2.97E-10	4.15E-11	4.96E-29	1.10E-30	8.63E-32
BAND 2 POWER	7.43E-06	1.32E-07	1.85E-11	4.94E-12	2.81E-13	1.13E-30	2.54E-32	5.76E-33
BAND 3 POWER	7.06E-07	1.19E-07	1.02E-11	1.96E-12	7.36E-14	7.04E-30	1.81E-31	2.07E-31
BAND 4 POWER	7.06E-07	1.19E-07	2.92E-11	5.76E-12	6.82E-14	1.04E-25	2.44E-27	1.30E-27
BAND 5 POWER	7.06E-07	1.19E-07	4.37E-11	8.03E-12	6.82E-14	3.90E-25	1.39E-26	7.69E-27
SOURCE ANG	5.0	20.0	40.0	64.0	100.0	124.0	130.0	150.0

Table 19 presents similar data to that presented in Table 18 except that the BRDF for the primary is represented by the worst mirror BRDF and has results 1000 times above those in Table 18.

Table 19 180 DEGREES AZIMUTH WORST MIRROR PERCENT OF POWER CONTRIBUTED BY EACH OBJECT AS A FUNCTION OF OFF AXIS SOURCE POSITION

OBJECTS/	OFF AXIS POSITION							
	1	2	3	4	5	6	7	8
16 PRI MIR	100.00	100.00	100.00	100.00	100.00	100.00	100.00	100.00
BAND 1 POWER	1.25E-03	1.19E-04	2.92E-09	9.04E-10	1.06E-10	1.88E-28	4.15E-30	3.24E-31
BAND 2 POWER	5.49E-03	5.18E-04	1.57E-08	3.86E-09	3.45E-10	1.98E-27	4.44E-29	8.35E-30
BAND 3 POWER	7.06E-04	1.19E-04	8.18E-09	1.49E-09	6.82E-11	6.87E-27	1.76E-28	1.93E-28
BAND 4 POWER	7.06E-04	1.19E-04	2.92E-08	5.76E-09	6.82E-11	1.04E-22	2.44E-24	1.30E-24
BAND 5 POWER	7.06E-04	1.19E-04	4.37E-08	8.03E-09	6.82E-11	3.90E-22	1.39E-23	7.69E-24
SOURCE ANG	5.0	20.0	40.0	64.0	100.0	124.0	130.0	150.0

Table 20 represents the contributions from a diamond turned primary mirror (#4 in Table 17).

Table 20 180 DEGREES AZIMUTH DIRBE DIAMOND TURNED MIRROR
PERCENT OF POWER CONTRIBUTED
BY EACH OBJECT AS A FUNCTION
OF OFF AXIS SOURCE POSITION

OBJECTS/	OFF AXIS POSITION							
	1	2	3	4	5	6	7	8
16 PRI MIR	100.00	100.00	100.00	100.00	100.00	100.00	100.00	100.00
BAND 1 POWER	1.17E-01	2.89E-03	5.77E-08	2.88E-08	4.26E-09	5.36E-27	1.18E-28	9.25E-30
BAND 2 POWER	7.06E-04	1.19E-04	4.23E-09	9.18E-10	7.30E-11	4.73E-28	1.06E-29	1.98E-30
BAND 3 POWER	3.93E-04	6.63E-05	4.69E-09	8.27E-10	3.80E-11	3.82E-27	9.78E-29	1.07E-28
BAND 4 POWER	9.63E-06	1.62E-06	3.99E-10	7.85E-11	9.30E-13	1.42E-24	3.33E-26	1.77E-26
BAND 5 POWER	3.04E-06	5.13E-07	1.89E-10	3.46E-11	2.94E-13	1.68E-24	5.99E-26	3.31E-26
SOURCE ANG	5.0	20.0	40.0	64.0	100.0	124.0	130.0	150.0

The PST data for the 180 degree azimuth, Tables 5, 7, 8, 9, and 10, were utilized to calculate the image plane irradiance due to a hemispherical source of uniform brightness. In the analysis the hemisphere, faceted into 40,000 segments, was 1.E6 mm (system units) in radius and was emitting 1.E-6 watts/sq. mm. The detector irradiance for these input conditions is shown in Table 21.

Table 21. The image plane irradiance due to a hemisphere radiating at 1E-6 watts/sq. mm.

DETECTOR IRRADIANCE	
BAND 1	.27E-11 watts/sq. mm.
BAND 2	.368E-13 watts/sq. mm.
BAND 3	.270E-14 watts/sq. mm.
BAND 4	.388E-14 watts/sq. mm.
BAND 5	.746E-14 watts/sq. mm.

The PSNIT PLOTS for each study, except the thermal case, are shown in Figures 19 through 23.

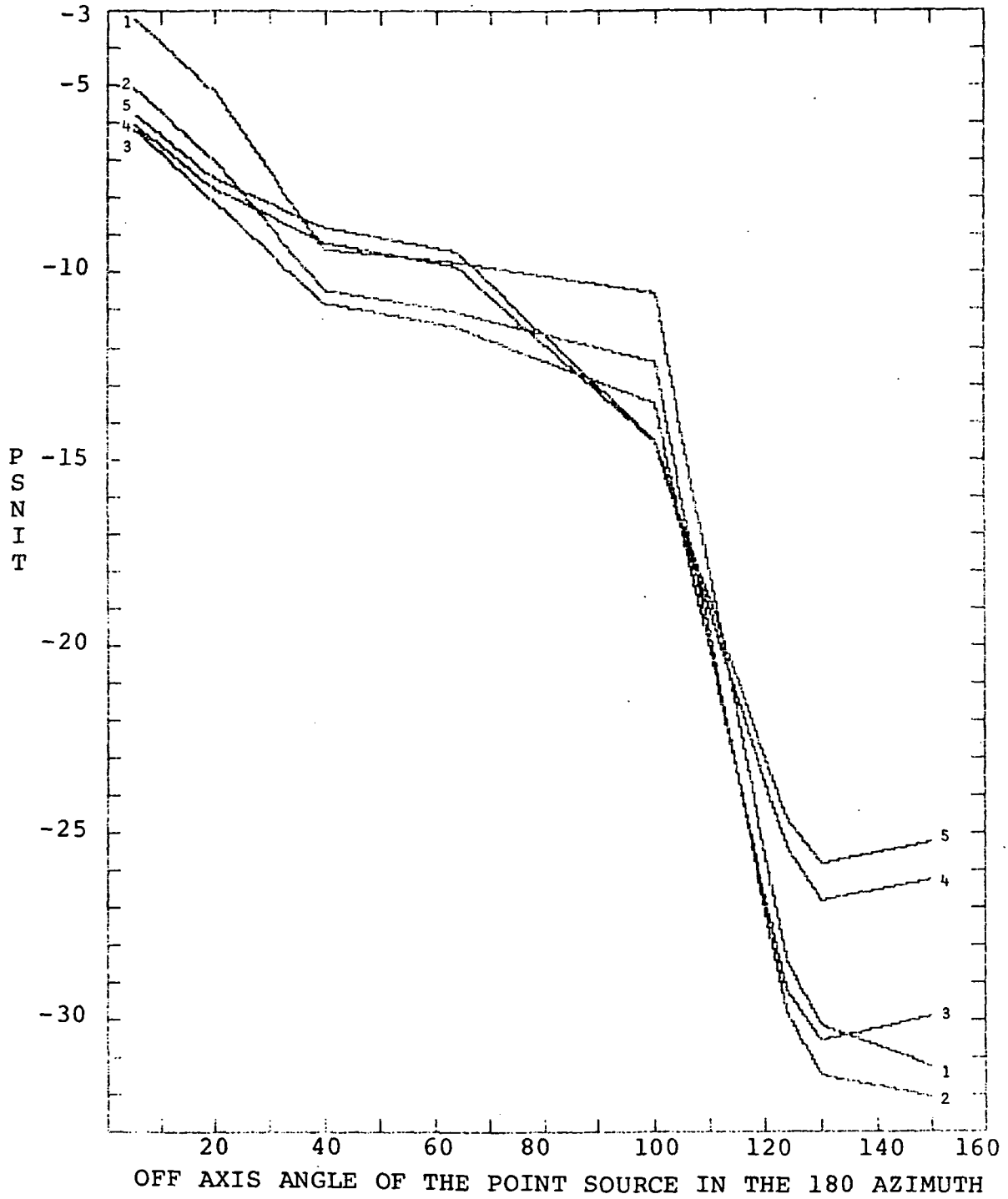

Figure 19. Nominal case 180 degree azimuth.

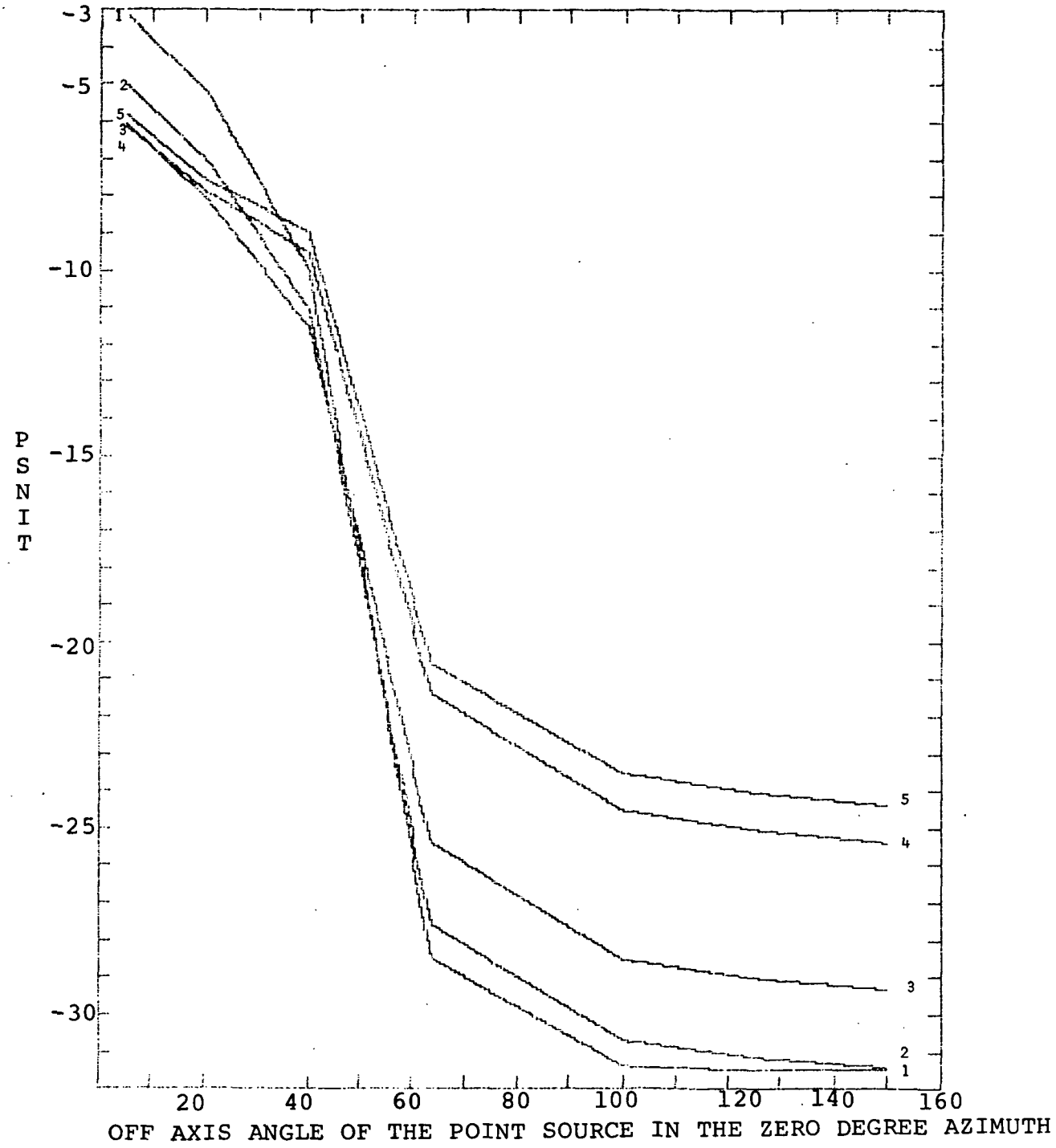

Figure 20. Nominal case zero degree azimuth.

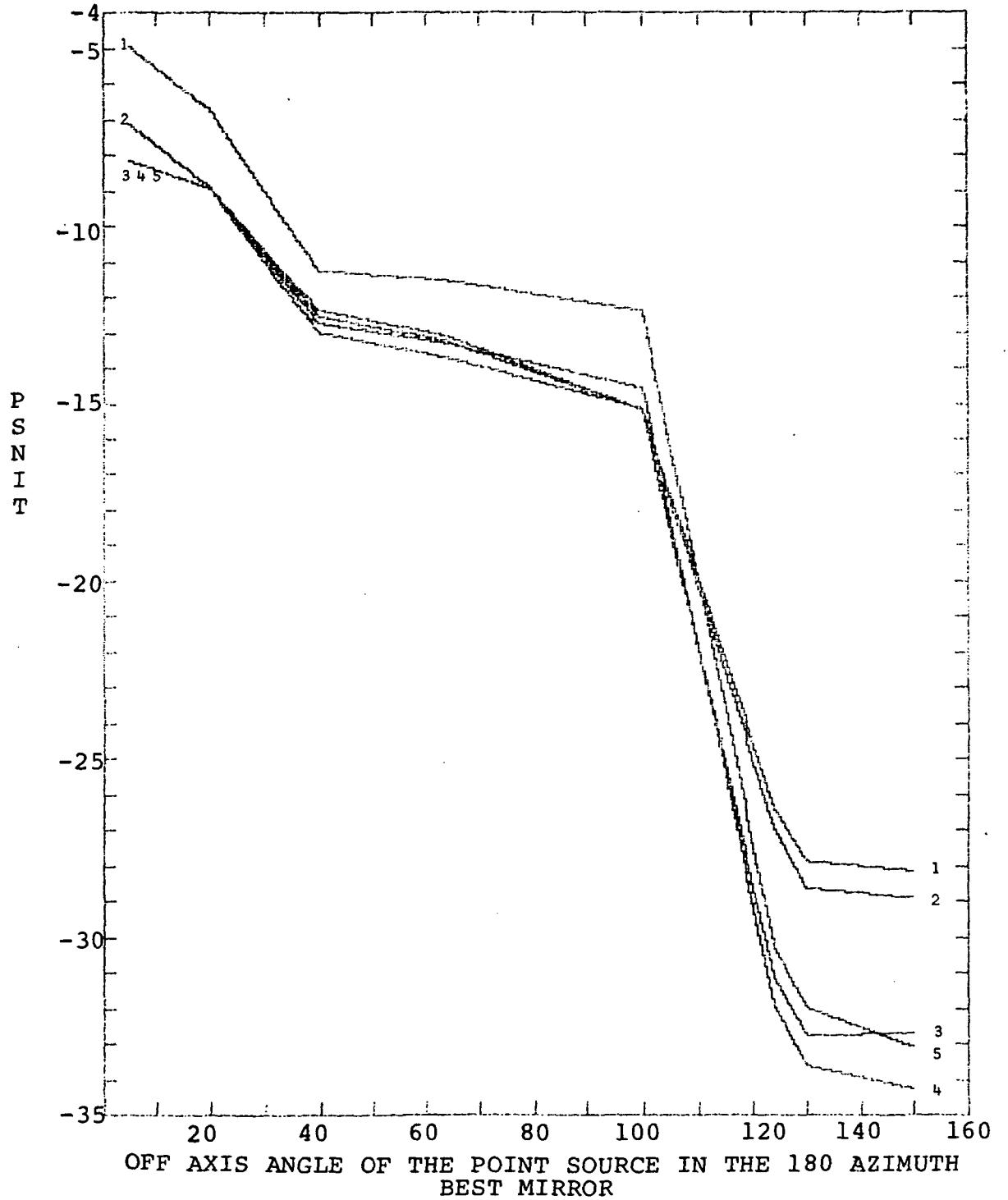

Figure 21. Best mirror only PSNIT, 180 degree azimuth.

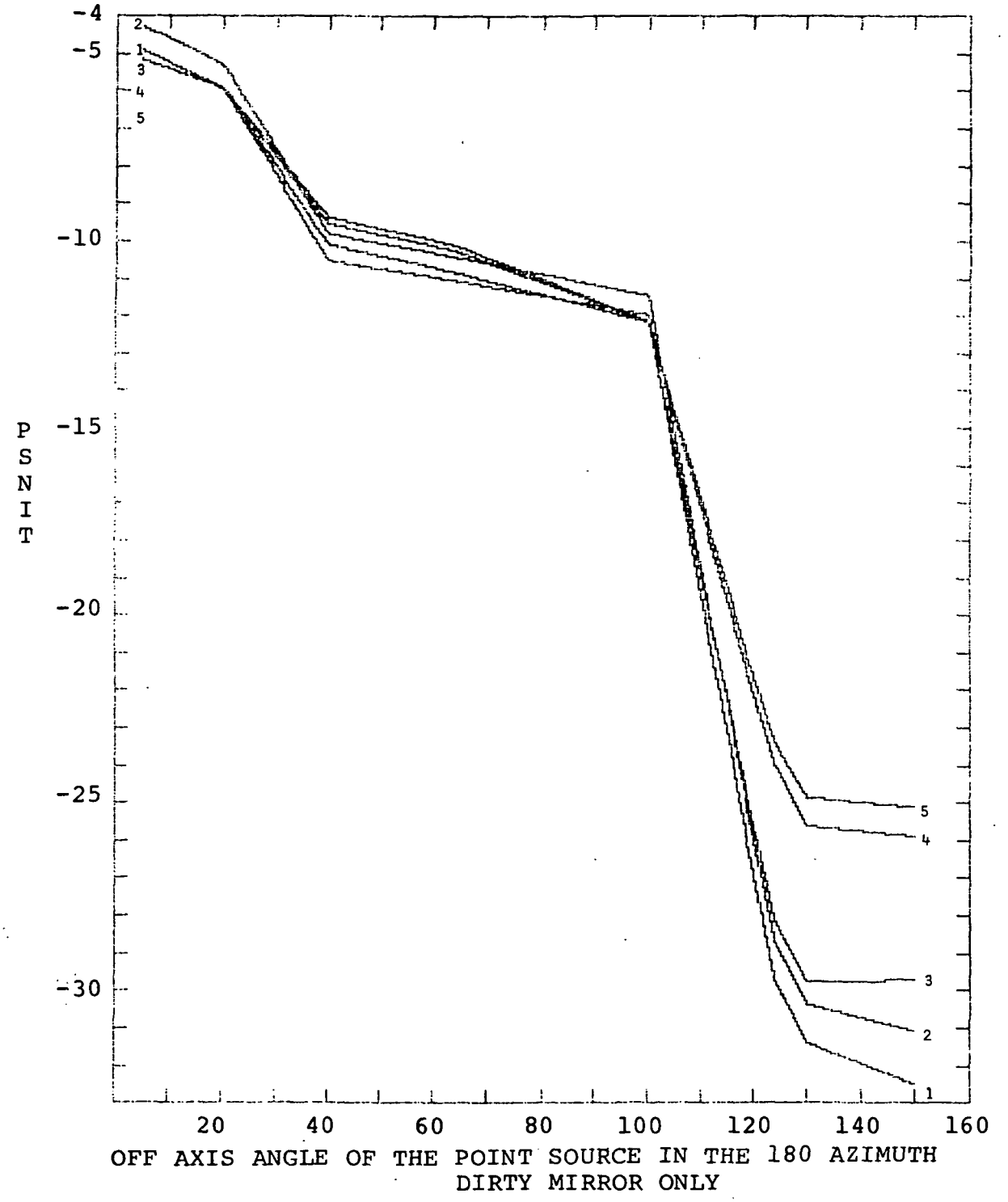

Figure 22. Dirty mirror only PSNIT, 180 degree azimuth.

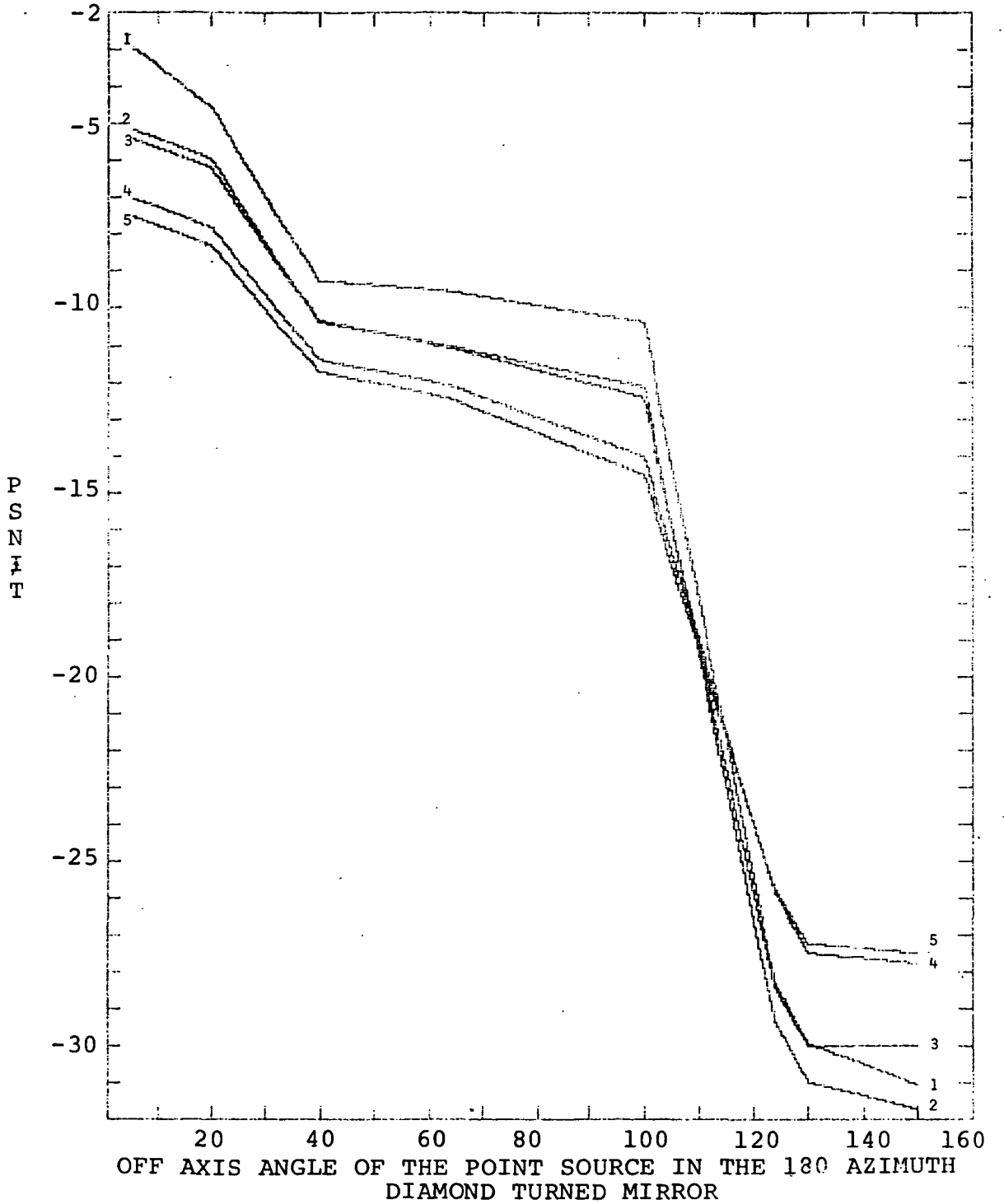

Figure 23. Diamond turned mirror only PSNIT, 180 degree azimuth.

6.0 CONCLUSIONS/RECOMMENDATIONS

The results show that DIRBE is basically well designed. Other than the one design feature that causes the diffraction to be higher than is necessary at the long wavelengths the results show that no major redesign will be necessary. All the straylight problems are tied to the performance of the primary mirror in the shorter wavelength bands, or to the constant phase diffraction due to the alignment of the diffracting edge in the upper bands. The specular nature of Martin Black at the long wavelength also plays a role.

The diffraction problem can easily be solved by reducing the clear aperture size of FS2 or by increasing the size of FS1. Either of these changes would make the image of FS1, hence its diffraction, fall further away from the edge of FS2. This would reduce the diffraction by approximately

$$R(\theta)^{-X}$$

$R(\theta)$ is the ratio $R(\theta) = \theta/\theta_o$

θ is the angular difference from the point on FS2, that is the conjugate image point of a source on FS1, to the edge of FS2.

θ_o is the presently designed angular difference, approximately .05 degrees.

x is a value, either 2 or 3 depending on whether, respectively there is a constant phase or just a stationary phase contribution from the edge.

This exponential fall off can be used to reduce the diffraction at all wavelengths, but most importantly in bands 4 and 5 at all off axis angles.

The choice of either increasing FS1 or decreasing FS2 is not equivalent. Increasing FS1 would keep the Point Source Transmittance (PST) much higher for sources very near the edge of FOV. The focused power would slip through the bigger hole (FS1) and fall directly onto FS2. Then with one single diffraction it would reach the chopper. If FS1 remains the same, and FS2's aperture size is reduced, then the FOV is effectively smaller. For DIRBE the later seems to be the more desirable choice.

APART calculated 33 specular paths that involved radiation from object 6, the forebaffle, to object 11 the main baffle, and then onto the primary. This causes a great increase in the power loaded onto the primary. If the

long wavelength diffraction is significantly reduced, then this problem with Martin Black will be significant. Several groups are working on a diffuse black that will retain its diffuse characteristics over a broad band. One that would be suitable for the DIRBE and SIRTF missions. To improve DIRBE in Bands 4 and 5 it appears necessary to both change the sizes of one or more apertures and to change the black coating on the vanes. This analysis used Martin Black as the black coating for several reasons. It was specified because it was the only black for which we had legitimate BRDF data in bands 2 and 4. It is assumed that the BRDF in band 3 was similar to band 2, and band 5 was similar to band 4.

The BRDF of the primary mirror is a very major concern and deserves additional attention. It should be clear that in the present design its scatter dominates. It should be recognized that if the above field stop changes are implemented, the scatter from the primary will dominate in all the bands. Therefore, special care should be taken during polishing to assure that the BRDF of the bare substrate cannot be substantially improved. Explicitly this means making periodic BRDF measurements on the bare substrate, and plotting the decrease in the BRDF as the polish time is increased. Second, before coating, the surface should be visually inspected with a low power microscope, about 30x, and a high intensity lamp. Eyeball inspection with a high intensity lamp is not a valid test. The above two procedures should be required.

The cleaning of the substrate prior to coating can be the last crucial step in the process. Hopefully any contamination of the primary after the mirror is coated will be able to be removed. On the other hand, contamination of the primary before coating can only be corrected by stripping the coating off and recoating it carefully. It is assumed that the following procedures will be done in a suitable clean room environment.

The recommended procedure, or some variation of it, is as follows. The mirror should be washed in a soap bath, and the dried with a large sheet of lintless paper or cloth. At this stage the tissue or cloth will not produce any adverse affects on the surface. Blow drying the surface will leave many pockets of contaminants on the surface. After the mirror is dry, a collodion coating is applied to the entire surface according to the suppliers instructions. After the coating has solidified it can be removed from the surface. Care must be taken so that the entire coating of collodion is removed in one piece. If it isn't, special steps will have to be taken to pick up any residual pieces. The collodion will remove many, many more particulates than any other known method. However, the collodion will leave behind an invisible layer that will not allow a thin film coating of gold (or aluminum) to adhere to the substrate properly. Subsequent cleaning of the coated surface could remove substantial portions of the coating, like 15 to 30% of the surface area. Therefore the mirror must now be cleaned one final time. This step is not unlike the first step. The surface is washed by dragging a large sheet of lintless paper (or cloth) soaked in either a very clean grade of acetone, or alcohol. The collodion has removed most of the particulates so the pooling or streaking of the mirror by such particulates should be minimized. This step will remove the thin layer that the collodion left behind and therefore, allow a thin film coating to adhere to the substrate. Inspection of the surface should reveal

almost no visible contamination.

The coating of the mirror can now be done with confidence. After the mirror is removed from the coating chamber one can expect, and even watch, the room's contaminates be attracted to the virgin surface. At this stage the BRDF of the mirror should be measured within 30 minutes. This will set, what hopefully will be, the performance goal for the primary mirror. There shouldn't be any great concern about the contamination of the primary at this stage. It's going to get dirty sometime prior to launch. It can be cleaned, hopefully, if not right back to the measurement made just after it was removed from the chamber.

The only method that can be used to clean the coated mirror is with the collodion. From this point on there is no lintless paper or cloth, and no alcohol, water, or acetone. You will have to "buy" the invisible layer of contaminant left by the collodion. It should not affect the performance. Any cloth, or tissue laid on the coated surface will scar the coating and may adversely affect the BRDF, especially in the shorter wavebands.

NASA should make plans that allow for the re-cleaning of the primary as late, and as close to the launch date as possible. By this stage the BRDF of the primary should have degraded by one to two orders in magnitude. Depending on the design, and the re-alignment procedures, it might take as long as 4 weeks to reclean the mirror. It will be necessary, and it will be beneficial in terms of system performance. From this point on any contamination will go with the primary into space, and most likely will stay on the primary forever more.

The use of vanes on a baffle surface can greatly reduce the amount of power propagated to the detectors. The optimum design is dependent upon the vane depth, spacing, the angular range that the unwanted source can be positioned, and the direction of the collector of the vane scattered energy. In DIRBE the collector is the primary mirror. The unwanted source of energy is the Forebaffle, a fixed position, and the dark sky or other sources that can put power on the baffles over a wide range of angles. The important range of angles for the baffles for a specific source is from the point where the power of this source just misses putting power on the primary to the position where it can no longer put power on the baffles directly. For this range of angles there should be no direct path from the source to the walls (the bottom of the vane structure) that can scatter directly to the primary mirror. DIRBE, as analyzed has no such paths. Instead, in DIRBE, the vanes are so close together that the side walls almost never receive any direct power - an over design feature that adds unnecessary weight and increases the scatter slightly. There are more edges that can directly scatter power to the primary, and the solid angle that the backside of the preceding vane, in a vane cavity, subtends is larger when the vanes are closely spaced. The difference in the performance is not all that significant in the DIRBE design unless the weight is important. The vanes can either be moved further apart, or the depth of the vanes reduced. The more desirable one is to keep the vane depth and increase the spacing. In any change made there must not be a direct path from the source to the wall to the primary.

7.0 SUMMARY

The DIRBE analysis implies that the performance of the system is controlled by two features. First and foremost it is controlled by the design of the optical/baffle system, i.e the "z" type system with the field stops and Lyot stops, and the up front forebaffles and vane structure. That is already there, albeit perhaps over designed. If it can be assembled as designed there is no need to make major changes. Only relatively minor modifications are suggested.

The second major performance feature, and the current controlling factor, is the BRDF of the primary. The system's performance appears to have a linear relationship to the primary's BRDF characteristic. It will warrant every bit of attention during fabrication and needs to be kept clean.

APPENDIX A

TABLE 1A. ONE REPRESENTATIVE SET OF INPUT DECKS

```
*  DECK FOR DIRBE
* UNITS MM, AXIS TILTED 30 DEG TO OPTICAL AXIS OF OBJECT SPACE
* INPUT DECK IS CALLED DIRBE
* JUL 25 1983
*    STRAYLIGHT ANALYSIS
*    - NOMINAL DESIGN
*    DIFFRACTION ANALYSIS
*    THERMAL EMISSION ANALYSIS
PLOT 0 300.
Y-YBAR PLOT
COATING BAFFLES .01
COATING OPTICS .001 -1.5
EDGE 1 1 1 -298.14 2031.20 =SUNSHIELD
       ROTATE X 30.
       SHIFT Y 149.07
EDGE 2 1 1 -299.30 2006.20 =2ND DIF EDG
       ROTATE X 30.
       SHIFT Y 149.65
EDGE 3 -1 1 -298.14 1981.20  =IN RAD EDG
       ROTATE X 30.
       SHIFT Y 149.07
CONE 4 -1 4 -298.14 1981.20 -55. 1879.60 =RADIATOR
       ROTATE X 30.
       SHIFT Y 149.07
EDGE 5 -1 1 -55. 231.459  =FOREBAFE EDGE
       XFACTOR .714
       ROTATE X 30. 0.0 .001
       SHIFT Y 2.
CONE 6 -1 4 -55. 231.459 0. 136.179 =FOREBAFF
       XFACTOR .714 .892
       ROTATE X 30 0. .001
       SHIFT Y 2.0
EDGE 33 -1 1 0. 136.179 =FOREBAFF REAR EDGE
       XFACTOR .892
       ROTATE X 30 0. .001
       SHIFT Y 2.
CONE 7 -1 1 -68.10 115.95 -52.64 116.0   =OSSP1 5
       SLICE BACK -30.
       SLICE FRONT -30.
CONE 8 -1 5 -40.57 110. 66.25 110. =OSSP6-24
       SLICE BACK -30.
EDGE 9 -1 1 69.28 107.5  =OSSP EDGE
CONE 10 -1 3 69.28 107.5 139.28 107.5 =OUTER MAIN TUBE
CONE 11 -1 5 139.28 107.5 294.28 107.5 =MAIN TUBE
       SLICE NORMAL Z 102.9 90. 0. -71.07 294.28
CONE 34 -1 2 294.28 107.5 369.28 107.5 =RT MAIN BAF
       SLICE NORMAL Z 136.72 90. 0. 8.56 369.28
DISK 12 -1 2 398.78 128.5 155. =TBAFF
```

TABLE 1A (cont.)

```
       ROTATE X -4.0
       SHIFT Y 2.0
DISK 13 -1 3 421.54 112.5 135.0 =PRI M BAF
       ROTATE X -12. 0. 456.54
CONE 14 -1 1 421.54 111.5 446.54 111.5 =MINI VANES
       ROTATE X -11.77
       SHIFT Y 2.0
EDGE 15 -1 1 446.54 107.5 =PRI DIF ED
       ROTATE X -11.77
       SHIFT Y 2.0
CONE 17 -1 6 77.73 15. 339.4 105.91 =LOWER MAIN
       SLICE NORMAL Z -100.65 90. 0. -.22 339.4
       ROTATE X -23.54 0. 456.54
       SLICE BACK -23.55
CONE 38 -1 2 339.4 105.91 385.42 121.9 =RT LOW MAIN
       SLICE NORMAL Z -66.83 90. 0. -.22 339.4
       ROTATE X -23.54 0. 456.54
DISK 16 -1 7 456.54 115.0 =PRI MIR
   OPTIC
   CC -1
   RD -892.14
       ROTATE X -11.77
REPEAT 14 11 10 17
PYRAMID 18  -1 3 10.68 6.276 85.68 21.84  =PFTA
       SLICE FRONT 23.55
*  PFTA= PRIME FOCUS THROAT ASSEMBLY
STREDGE 20 -1 3 -3.96  3.96 10.68 3.96 3.96 10.68 =TOP F1
STREDGE 21 -1 3 3.96  3.96 10.68 3.96 -3.96 10.68 =RT F1
STREDGE 22 -1 3 3.96  -3.96 10.68 -3.96 -3.96 10.68 =BOT F1
STREDGE 23 -1 3 -3.96  -3.96 10.68 -3.96 3.96 10.68 =LEF F1
CONE 32 -1 5 10.68 8.0 -136.31 55. =SEC MIR BAFFLE
       SLICE NORMAL Z 66.80 90. 0. 55. -136.31
CONE 39 -1 4 -136.31 55. 1.605 24. =LOW BAF SEC-F1
       SLICE NORMAL Z -100. 90. 0. 24. 1.605
       ROTATE X 16.168
DISK 28 1 6 -136.31 45. =SEC MIR
   OPTIC
   CC -.2899159
   RD 293.978
       ROTATE X 8.084
REPEAT 32 39
EDGE 29 -1 1  1.605 23. =PUPIL2
       XFACTOR .957
       ROTATE X -16.79
PYRAMID 30 -1 5 -5.974 26.25 332.3 14.596  =PYR SEC
       SHIFT Y -1.25
       SLICE BACK 16.77
STREDGE 24 -1 3 -11.04 11.04 332.3 11.04 11.04 332.3 =TOP F2
STREDGE 25 -1 3 11.04 11.04 332.3 11.04 -11.04 332.3 =RT F2
STREDGE 26 -1 3 11.04 -11.04 332.3 -11.04 -11.04 332.3 =BOT F2
STREDGE 27 -1 3 -11.04 -11.04 332.3 -11.04 11.04 332.3 =LEF F2
PYRAMID 35 -1 6 332.3 12.04 595. 43.68  =TERT CONE
       SLICE FRONT 48.
```

TABLE 1A (cont.)

```
PYRAMID 37 1 4 613. 43.68 516.58 43.68   =BOT
       SLICE NORMAL Z -64. 90. 0. 43.68 613.
       ROTATE X -5.73  0. 613.1
       SHIFT Y -45.7
DISK 36 -1 4 610.1 52.5 =TER MIR
   OPTIC
   CC -.10044
   RD -2000.6571
       ROTATE X -12.91
REPEAT 35 37
RECT 98 1 3 481.52 0.  9.0 1.0 =IMAGE CHOP
       ROTATE X 24.76
XEQ
DIRECTION X
PLOT 0 300.
END
```

TABLE 2A.

```
*  DECK FOR DIRBE
* UNITS MM, AXIS TILTED 30 DEG TO OPTICAL AXIS OF OBJECT SPACE
* INPUT DECK IS CALLED DIRBE
* JUL 25 1983
*    STRAYLIGHT ANALYSIS
*    - NOMINAL DESIGN
*    DIFFRACTION ANALYSIS
*    THERMAL EMISSION ANALYSIS
POINT SOURCE ANGLES 5.  20. 40. 64. 100. 124. 130. 150.
POINT SOURCE AZIMUTH 180.
LIST FILES
PRINT HEADING DIST ANGLE 0
S .01 1.01
S .01 2.01
   H 1.01
S .01 3.01
   H 1.01
S .01 6.01
   H -4.01
S .01 7.01
   H -4.01 -6.01
S .01 8.01
   H -4.01 -6.01
S .01 9.01
   H -3.01 -6.01 6.01
S .01 10.01
   H -10.01 -6.01 -4.01
S .01 11.01
           SECTION LENGTHS COLLECTOR 25 30 30 30 40
   H -10.01 -6.01 -4.01
S .01 34.01
           SECTION LENGTHS COLLECTOR 50. 25.
   H -10.01 -6.01 -4.01
S .01 14.01
   H -10.01 -6.01 -4.01
S .01 15.01
   H -10.01 -6.01 -4.01
S .01 16.01
   H -10.01 -6.01 -4.01
S .01 17.01
   H -10.01 -6.01 -4.01 10.01
S .01 38.01
   H -10.01 -6.01 -4.01 10.01
S .01 17.02
   H -10.01 -6.01 -4.01
S .01 18.02
   H -10.01 -6.01 -4.01
S .01 4.01
   H -4.01
S 10.01 15.01
S 10.01 16.01
S 1.01 2.01
S 2.01 3.01
```

TABLE 2A.(cont.)

```
S 3.01 6.01
   H -6.01
S 3.01 5.01
S 6.01 11.01
           SECTION LENGTHS COLLECTOR 25 30 30 30 40
S 6.01 10.01
S 7.01 11.01
           SECTION LENGTHS COLLECTOR 25 30 30 30 40
S 7.01 10.01
   H -8.01
S 8.01 15.01
   H -10.01
S 8.01 16.01
   H -10.01
S 5.01 10.01
   H 6.01
S 5.01 11.01
           SECTION LENGTHS COLLECTOR 25 30 30 30 40
   H 6.01
S 9.01 15.01
S 9.01 16.01
S 11.01 16.01
           SECTION LENGTHS SOURCE 25 30 30 30 40
S 11.01 15.01
           SECTION LENGTHS SOURCE 25 30 30 30 40
S 17.01 15.01
S 17.01 16.01
S 34.01 16.01
           SECTION LENGTHS SOURCE 50. 25.
S 4.01 5.01
   THERMAL
S 4.01 6.01
   THERMAL
   H -6.01
S 15.01 20.02
PI SECTIONS COLLECTOR 3
S 15.01 21.02
S 15.01 22.02
S 15.01 23.02
S 20.02 29.03
PI SECTIONS SOURCE 3
PI SECTIONS COLLECTOR 6
S 21.02 29.03
S 22.02 29.03
S 23.02 29.03
S 29.03 24.03
PI SECTIONS SOURCE 6
PI SECTIONS COLLECTOR 3
S 29.03 25.03
S 29.03 26.03
S 29.03 27.03
S 24.03 98.04
PI SECTIONS 3
```

TABLE 2A (cont.)

```
S 25.03 98.04
S 26.03 98.04
S 27.03 98.04
S 16.02 98.04
PI SECTIONS SOURCE 6
S 14.01 16.01
      PI SECTIONS 6
S 10.01 14.01
S 20.02 98.04
PI SECTIONS  3
S 21.02 98.04
S 22.02 98.04
S 23.02 98.04
END
```

TABLE 3A

```
*  DECK FOR DIRBE
* INPUT DECK IS CALLED DIRBE
* JUL 25 1983
*    STRAYLIGHT ANALYSIS 180 DEG AZIMUTH
*    - NOMINAL DESIGN
*    DIFFRACTION ANALYSIS
EDGE RADIUS .002
UNITS MM
EARTH TEMPERATURE 230.
BANDWIDTHS
  1.0 1.5
  8.0 15.0
  37.5 38.5
  120. 200.
  200. 300.
THERMAL
  4 162.0 .025 2
WAVELENGTH 1.25
COATING 1 1.
COATING 2 MBLACK
COATING 3 CHEMGLAZ
COATING 4 MIRROR .01 SLOPE -2. BASE WAVELENGTH 10.6 MIN BRDF 1.E-8
COATING 5 120. 10. 34.0 .01 110. =OBJ 8
COATING 6 90. 10. 37. .01 107.5 =OBJ 10
COATING 7 90. 2.5 25. .01 123.75 =OBJ 13
COATING 8 GODDARDB
COATING 9 MIRROR .01 SLOPE -1.5 BASE WAVELENGTH 10.6 MIN BRDF 1.E-8
COATING 10 EDGE KIRCHOFF
COATING 11 90. 10. 10. .01 12.54 =OBJ 18
COATING 12 90. 10. 10. .01 16.26 =OBJ 18
COATING 13 90. 50. 37. .01 107.5 =OBJ 34
COATING 14 90. 25. 37. .01 107.5 =OBJ 34
COATING 15 90. 10. 10. .01 19.98 =OBJ 18
COATING 16 113.54 10. 16. .01 28.36 =OBJ 17
COATING 17 113.54 10. 16. .01 55.09 =OBJ 17
COATING 18 113.54 10. 16. .01 81.81 =OBJ 17
COATING 19 113.54 10. 16. .01 108.54 =OBJ 38
COATING 20 90. 45. 5. .01 20. =OBJ 35
COATING 21 83.13 12.5 4. .01 19.04 =OBJ 37
COATING 22 83.13 58. 4. .01 35.77 =OBJ 37
COATING 23 90. 25. 37. .01 107.5 =OBJ 11
COATING 24 90. 30. 37. .01 107.5 =OBJ 11
COATING 25 90. 40. 37. .01 107.5 =OBJ 11
COATING 26 120. 5. 22. .01 116. = OBJ 7
SURFACE 1  10
SURFACE 2  10
SURFACE 3  10
SURFACE 4  9
SURFACE 5 10
SURFACE 6  9
SURFACE 7  26
SURFACE 8  5
SURFACE 9  10
```

TABLE 3A (cont.)

```
SURFACE 10  6
SURFACE 11  23 3*24 25
SURFACE 13  7
SURFACE 14  8
SURFACE 15  10
SURFACE 16  4
SURFACE 17  16 16 17 17 18 18
SURFACE 18  11 12 15
SURFACE 19  10
SURFACE 20  10
SURFACE 21  10
SURFACE 22 10
SURFACE 23 10
SURFACE 24 10
SURFACE 25 10
SURFACE 26 10
SURFACE 27 10
SURFACE 28  4
SURFACE 29  10
SURFACE 34  13 14
SURFACE 35  20
SURFACE 36  4
SURFACE 37  3*21 3*22
SURFACE 38  19
SURFACE 98  1
SURFACE 99  1
PERCENT
STORE PERCENT 1
NOSHOW
RADIM 10.16
ICYSTOP 8
PLOTNUM 1
PSTPLOT PSNIT
PATHS
99
15 16
20 21 22 23 98
29
24 25 26 27
98
XEQ 2
PATHS
99
9 10 11 17
15 16
20 21 22 23 98
29
24 25 26 27
98
XEQ
PATHS
99
9 10
```

TABLE 3A (cont.)

```
15 16
20 21 22 23 98
29
24 25 26 27
98
XEQ
PATHS
99
8
15 16
20 21 22 23 98
29
24 25 26 27
98
XEQ
PATHS
99
1
2
3 4
5 6
10 11
15 16
20 21 22 23 98
98
XEQ 8
PERCENT
WAVELENGTH 10.6
STORE PERCENT 2
NOSHOW
RADIM 10.16
ICYSTOP 8
PLOTNUM 2
PSTPLOT PSNIT
PATHS
99
14 15 16
16 20 21 22 23 98
29 98
24 25 26 27
98
XEQ 2
PATHS
99
9 10 11 17
15 16
20 21 22 23 98
29
24 25 26 27
98
XEQ
PATHS
99
```

TABLE 3A (cont.)

```
9 10
15 16
20 21 22 23 98
29
24 25 26 27
98
XEQ
PATHS
99
8
15 16
20 21 22 23 98
29
24 25 26 27
98
XEQ
PATHS
99
1
2
3 4
5 6
10 11
15 16
20 21 22 23 98
98
XEQ 8
PERCENT
WAVELENGTH 38.0
STORE PERCENT 3
NOSHOW
RADIM 10.16
ICYSTOP 8
PLOTNUM 3
PSTPLOT PSNIT
PATHS
99
15 16
20 21 22 23 98
29
24 25 26 27
98
XEQ 2
PATHS
99
9 10 11 17
15 16
20 21 22 23 98
29
24 25 26 27
98
XEQ
PATHS
```

TABLE 3A (cont.)

```
99
9 10
15 16
20 21 22 23 98
29
24 25 26 27
98
XEQ
PATHS
99
8
15 16
20 21 22 23 98
29
24 25 26 27
98
XEQ
PATHS
99
1
2
3 4
5 6
10 11
15 16
20 21 22 23 98
98
XEQ 8
PERCENT
WAVELENGTH 160.
COATING 1 1.
COATING 2 MBLACK
COATING 3 CHEMGLAZ
COATING 4 MIRROR .01 SLOPE -2. BASE WAVELENGTH 10.6 MIN BRDF 1.E-8
COATING 5 VANES ANG 120. SEP 10. HEIGHT 34.0 RHO .01 RADIUS 110.
   SPECULAR MARTIN =OBJ8
COATING 6 VANES ANG 90. SEP 10. HEIGHT 37. RHO .01 RADIUS 107.5
   SPECULAR MARTIN =OBJ 10
COATING 7 VANES ANG 90. SEP 2.5 HEIGHT 25. RHO .01 RADIUS 123.75
   SPECULAR MARTIN =OBJ 13
COATING 8 GODDARDB
COATING 9 MIRROR 1 SLOPE -1.5 BASE WAVELENGTH 10.6 MIN BRDF 1.E-6
COATING 10 EDGE KIRCHOFF
COATING 11 VANES ANG 90. SEP 10. HEIGHT 10. RHO .01 RADIUS 12.54
   SPECULAR MARTIN =OBJ 18
COATING 12 VANES ANG 90. SEP 10. HEIGHT 10. RHO .01 RADIUS 16.26
   SPECULAR MARTIN =OBJ 18
COATING 13 VANES ANG 90. SEP 50. HEIGHT 37. RHO .01 RADIUS 107.5
   SPECULAR MARTIN =OBJ 34
COATING 14 VANES ANG 90. SEP 25. HEIGHT 37. RHO .01 RADIUS 107.5
   SPECULAR MARTIN =OBJ 34
COATING 15 VANES ANG 90. SEP 10. HEIGHT 10. RHO .01 RADIUS 19.98
   SPECULAR MARTIN =OBJ 18
```

TABLE 3A (cont.)

```
COATING 16 VANES ANG 113.54 SEP 10. HEIGHT 16. RHO .01 RADIUS 28.36
COATING 17 VANES ANG 113.54 SEP 10. HEIGHT 16. RHO .01 RADIUS 55.09
COATING 18 VANES ANG 113.54 SEP 10. HEIGHT 16. RHO .01 RADIUS 81.81
COATING 19 113.54 10. 16. .01 108.54 =OBJ 38
COATING 20 VANES ANG 90. SEP 45. HEIGHT 5. RHO .01 RADIUS 20.
   SPECULAR MARTIN =OBJ 35
COATING 21 VANES ANG 83.13 SEP 12.5 HEIGHT 4. RHO .01 RADIUS 19.04
   SPECULAR MARTIN =OBJ 37
COATING 22 VANES ANG 83.13 SEP 58. HEIGHT 4. RHO .01 RADIUS 35.77
   SPECULAR MARTIN =OBJ 37
COATING 23 VANES ANG 90. SEP 25. HEIGHT 37. RHO .01 RADIUS 107.5
   SPECULAR MARTIN =OBJ 11
COATING 24 VANES ANG 90. SEP 30. HEIGHT 37. RHO .01 RADIUS 107.5
   SPECULAR MARTIN =OBJ 11
COATING 25 VANES ANG 90. SEP 40. HEIGHT 37. RHO .01 RADIUS 107.5
   SPECULAR MARTIN =OBJ 11
COATING 26 VANES ANG 120. SEP 5. HEIGHT 22. RHO .01 RADIUS 116.
   SPECULAR MARTIN =OBJ 7
STORE PERCENT 4
NOSHOW
RADIM 10.16
ICYSTOP 8
PLOTNUM 4
PSTPLOT PSNIT
PATHS
99
15 16
20 21 22 23 98
29
24 25 26 27
98
XEQ 2
PATHS
99
9 10 11 17
15 16
20 21 22 23 98
29
24 25 26 27
98
XEQ
PATHS
99
9 10
15 16
20 21 22 23 98
29
24 25 26 27
98
XEQ
PATHS
99
8
```

TABLE 3A (cont.)

```
15 16
20 21 22 23 98
29
24 25 26 27
98
XEQ
PATHS
99
1
2
3 4
5 6
10 11
15 16
20 21 22 23 98
98
XEQ 8
PERCENT
WAVELENGTH 250.
STORE PERCENT 5
NOSHOW
RADIM 10.16
ICYSTOP 8
PLOTNUM 5
PSTPLOT PSNIT
PATHS
99
15 16
20 21 22 23 98
29
24 25 26 27
98
XEQ 2
PATHS
99
9 10 11 17
15 16
20 21 22 23 98
29
24 25 26 27
98
XEQ
PATHS
99
9 10
15 16
20 21 22 23 98
29
24 25 26 27
98
XEQ
PATHS
99
```

TABLE 3A (cont.)

```
8
15 16
20 21 22 23 98
29
24 25 26 27
98
XEQ
PATHS
99
1
2
3 4
5 6
10 11
15 16
20 21 22 23 98
98
OVERPLOT 1 2 3 4 5
XEQ 8
WAVELENGTH 10.6
COATING 1 1.
COATING 2 MBLACK
COATING 3 CHEMGLAZ
COATING 4 MIRROR .01 SLOPE -2. BASE WAVELENGTH 10.6 MIN BRDF 1.E-8
COATING 5 120. 10. 34.0 .01 110. =OBJ 8
COATING 6 90. 10. 37. .01 107.5 =OBJ 10
COATING 7 90. 2.5 25. .01 123.75 =OBJ 13
COATING 8 GODDARDB
COATING 9 MIRROR .01 SLOPE -1.5 BASE WAVELENGTH 10.6 MIN BRDF 1.E-8
COATING 10 EDGE KIRCHOFF
COATING 11 90. 10. 10. .01 12.54 =OBJ 18
COATING 12 90. 10. 10. .01 16.26 =OBJ 18
COATING 13 90. 50. 37. .01 107.5 =OBJ 34
COATING 14 90. 25. 37. .01 107.5 =OBJ 34
COATING 15 90. 10. 10. .01 19.98 =OBJ 18
COATING 16 113.54 10. 16. .01 28.36 =OBJ 17
COATING 17 113.54 10. 16. .01 55.09 =OBJ 17
COATING 18 113.54 10. 16. .01 81.81 =OBJ 17
COATING 19 113.54 10. 16. .01 108.54 =OBJ 38
COATING 20 90. 45. 5. .01 20. =OBJ 35
COATING 21 83.13 12.5 4. .01 19.04 =OBJ 37
COATING 22 83.13 58. 4. .01 35.77 =OBJ 37
COATING 23 90. 25. 37. .01 107.5 =OBJ 11
COATING 24 90. 30. 37. .01 107.5 =OBJ 11
COATING 25 90. 40. 37. .01 107.5 =OBJ 11
COATING 26 120. 5. 22. .01 116. = OBJ 7
PERCENT
STORE PERCENT 6
NOSHOW
RADIM 10.16
ICYSTOP 8
PLOTNUM 6
PSTPLOT PSNIT
```

TABLE 3A (cont.)

```
PATHS
99
15
20 21 22 23
29 98
24 25 26 27
98
XEQ 2
PATHS
99
9 10 11
15
20 21 22 23
29 98
24 25 26 27
98
XEQ
PATHS
99
9 10
15
20 21 22 23
29 98
24 26
98
XEQ
PATHS
99
8
15 16
20 21 22 23 98
29
24 25 26 27
98
XEQ
PATHS
99
1
2
3 4
5 6
10 11
15 16
20 21 22 23 98
98
OVERPLOT 2 6
END
```

FIGURE 12: MIRROR BRDF CHARACTERISTICS

APPENDIX B